The "Djedi" Robot Exploration of the Southern Shaft of the Queen's Chamber in the Great Pyramid of Giza, Egypt

• •

Robert Richardson

School of Mechanical Engineering, University of Leeds, UK
e-mail: R.C.Richardson@Leeds.ac.uk

Shaun Whitehead

Scoutek, Ltd, UK
e-mail: shaun@creationeer.co.uk

TC Ng

Independant researcher, Hong Kong

Zahi Hawass

Supreme Council of Antiquities, Egypt

Andrew Pickering

School of Mechanical Engineering, University of Leeds, UK

Stephen Rhodes

School of Computer Science, University of Manchester

Ron Grieve

Tekron, Canada

Adrian Hildred

Independant researcher, UK

Arjun Nagendran

Institute for Simulation and Training, University of Central Florida, USA

Jason Liu and William Mayfield

School of Mechanical Engineering, University of Leeds, UK

Mehdi Tayoubi and Richard Breitner

Dassault Systèmes, France

There are many unanswered questions regarding the construction and purpose of the Great Pyramid of Giza, Egypt. A climbing robot called "Djedi" has been designed, constructed, and deployed to explore shafts of the queen's chamber within the Great Pyramid. The Djedi robot is based on the concept of inchworm motion and is capable of carrying a long reach drill or snake camera. The robot successfully climbed the southern shaft of the Great Pyramid, deployed its snake camera, and revealed writing not seen for thousands of years. This paper details the design of the robot, including climbing steps in the shaft and lessons learned from experimental deployment. © 2013 Wiley Periodicals, Inc.

1. INTRODUCTION

Robots have the potential to explore parts of the Great Pyramid, Egypt that are inaccessible to humans, thereby revealing new information that can be used toward solving the many mysteries of pyramid construction. The robotic challenges for exploration of confined spaces are compact size while incorporating actuators and sensors for locomotion, tools, and data gathering. The Great Pyramid of Giza is the last remaining wonder of the ancient world. The pyramid, also known as the Pyramid of Khufu, is the largest pyramid in the Giza Necropolis archaeological site on the outskirts of Cairo, Egypt. It is known to house three chambers, including the queen's chamber (QC) and the king's chamber (KC). Two shafts leave the queen's chamber to head toward the north and south faces of the pyramid: the queen's chamber shaft north (QCN) and the queen's chamber shaft south (QCS), respectively. Each shaft is approximately 210 mm square, and after a short horizontal section of around 2 m

Direct correspondence to: Robert Richardson, e-mail: R.C.Richardson@Leeds.ac.uk.
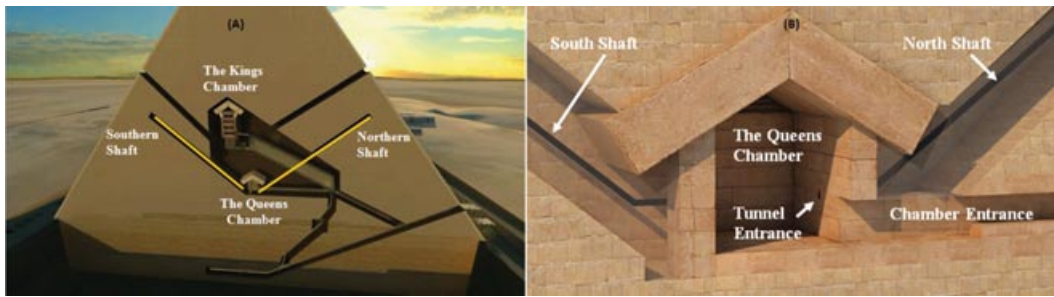
Figure 1. (A) Rendered cross-sectional image of the Great Pyramid illustrating the chambers along with the north and south shafts, each approximately 64 m long. (B) Rendered closeup illustration of the queen's chamber. (The shafts extend for approximately 64 m from the chamber toward the outer casing.)

Table I. A summary of the main theories for the purpose of the air shafts.

Suggested purpose	Description	Investigation
Light or Star shafts	For admitting light into the chamber, or for precisely pointing at particular stars or constellations	Alignment - do the shafts align with particular stars, on particular dates? Are they straight enough to allow light to enter? Any evidence of means to enhance reflection?
General spirit/soul shaft, i.e., model passages	A model passage for the pharaoh to ascend to the stars, not necessarily precisely orientated	Any hieroglyphic/symbolic evidence? Any other features of model passages?
Water shafts	e.g., for hydraulic purposes, such as lifting building blocks	Any evidence of water-tight sealing?
Ventilation shafts	–	–
"Energy" shafts	Some form of hydrogen power plant	Any evidence of sealing?
Acoustic communication shafts	For coordinating building effort as the pyramid reached the height of the king's chamber	Heights of the ends of the shafts with respect to each other
Celestial waterways	–	–
They lead to something	e.g., miniature serdabs?	Look for evidence of unusual constructions close to the end of the shafts. Inspect second blocking stones in each shaft. Drill and view beyond second blocking stones if safe and practical
A conduit	For something physical to leave the pyramid, such as smoke	Look for evidence of movable first/second blocking stones
Conduit into chamber	For something to be sent down to the chamber once it was complete	Look for evidence of movable first/second blocking stones
Other symbolic purpose	e.g., "magical" lengths	Do the shafts have equal lengths despite ascending at different angles/directions? Are the general dimensions consistent?

they rise at an angle of approximately 40° from the horizontal toward the north and south faces of the pyramid [Figure 1(A)]. The entrances to the shafts are positioned on the chamber walls [Figure 1(B)]. The queen's chamber is accessed through an entrance of sufficient size to allow a crouched human to enter. The shafts extend for approximately 64 m from the chamber toward the outer casing (as found from previous expeditions); however, these shafts mysteriously do not breach the outer casing, and their pur-

pose and construction remain one of the great mysteries of the pyramid.

The shafts are unique to the Great Pyramid, so any findings that help to determine their purpose will have significant archaeological value. Researchers have suggested many theories for the shafts, the more popular of which are alignment with the stars or that they lead to something. Table I lists the major theories along with investigations that will contribute to proving or disproving them. Historically, a

Figure 2. An image of the Upuaut Rover (Gantenbrink, 1999).

wide variety of methods have attempted to uncover secrets of the shafts, including observing the travel of smoke within the shafts and pushing long metal rods into the shafts. Recently, several robots have been developed to explore the shafts and provide direct video feedback of the shaft features.

1.1. Upuaut

Between 1991 and 1993, the German Archaeological Institute in Cairo (DAIK) and the Supreme Council of Antiquities (SCA) collaborated on the Upuaut Project to investigate the shafts. A small robot called Upuaut (Figure 2) was created by a German robotics expert, Rudolf Gatenbrink, to explore the shafts (Gantenbrink, 1999). The Upuaut robot consisted of two tracks forced apart through a lead screw system to create traction on the shaft walls. In March of 1993, Upuaut 2 was used to investigate the northern shaft in the QC (QCN). The robot was able to travel 19 m into the shaft, at which point the tunnel turned west at a 45° angle; Upuaut 2 was unable to navigate this turn. Upuaut 2 also explored the south of the QC (QCS). The robot traveled approximately 57 m into QCS, where it reached a 40-mm-high step. After careful manoeuvering, the robot was able to cross the step and advance forward. At about 63.5 m from the entrance to the tunnel, Upuaut 2 encountered a stone built across the shaft to terminate it. This stone has become known as the "first blocking stone" and had two "copper handles" mounted centrally of unknown purpose or function.

1.2. Pyramid Rover

In 2001, a new robot was created by iRobot, a robotics firm in Massachusetts, USA. The robot was named Pyramid Rover, and it consisted of two standard iRobot tracked chassis adapted to travel inside the QC shafts (Hawass, 2002). Compressed, it was 12 cm wide, 11 cm high, and 30 cm long. Pyramid Rover was able to grip the floor and ceiling with rubber tracks, and it was tethered to the controller computer with a cable. It was also equipped with lights, high-resolution video cameras, and an echo-impactor sensor. The robot was successful in traveling the full length of the southern tunnel (after abutting a ramp to the step) and drilled a hole in the first blocking stone. The robot used a camera to image directly behind the stone and discovered another stone later referred to as the second door. The robot also climbed the northern shaft, traversing the shaft bends, and discovered a door similar in appearance to that in the southern shaft.

1.3. Search for the Next Pyramid Exploration Robot—Djedi

Pyramid Rover did not provide a comprehensive view of the interior of the small "chamber" behind the first blocking stone in the QCS, as the camera could only look forwards toward the face of the second blocking stone. A visual survey of this space was considered to be the next essential step in determining the purpose of the shafts and blocking stones. After the completion of the Pyramid Rover expedition, the Supreme Council of Antiquities (SCA) decided to seek out a team that could accomplish two main tasks: (a) to send a robot to comprehensively examine the space beyond the first blocking stone of the QCS and drill a hole through the second stone to see what lies behind it, and (b) to send a robot through the QCN and drill a hole through its blocking stone to explore behind it. The SCA hence built a limestone practice tunnel in the desert, which provided an exact replica of the air shafts and their environment to find the robot that was best-suited for exploring the shafts. At the end of the trials, the team from Leeds University was chosen and the robot was called Djedi.

1.4. Knowledge from Previous Missions

Previous expeditions identified key features within the shaft. The southern shaft has a horizontal entrance of approximately 210 mm square and 2 m long. After 2 m of horizontal travel, the shaft transitions to a 40° incline. At approximately 30 m there is a lateral displacement of the shaft [Figure 3(A)] and at a distance of 59 m there is a 40 mm step on the floor [Figure 3(B)]. The surface of the shaft walls varies in consistency from smoothly polished stones to roughly cut and flaky, loose surfaces. At the top of the shaft, there is a limestone block (a blocking stone) of 60 mm approximate thickness. Behind the first blocking

Figure 3. Major obstacles within the southern shaft: (A) lateral displacement, (B) floor step (Gantenbrink, 1999).

stone is a small space of approximately 200 mm depth and an identical cross-section profile. Another stone surface, referred to as the second blocking stone, is at the end of the known shaft. Crucially, the tracks of previous robots marked the surface of the shaft walls; this is a result of the high normal forces implemented and skid steering of tracks.

A specification for the Djedi robot was created from knowledge of previous missions. The key features of the Djedi specification are as follows:

1. The tractive climbing force must be obtained with minimal or no damage to the pyramid walls. A peak safe traction force is unknown, but this requirement precludes the use of lead screws and tracks which have been proven to damage the shaft walls.
2. The shaft cross-sectional area is defined conflictingly within the literature, however the predicted shaft width and height range between 200 and 240 mm.
3. The robot must be capable of traveling between the horizontal and 40° inclined section of the shaft, which occurs at approximately 2 m into the shaft. This places restrictions on the robot length and height.
4. The robot must be able to hold its position rigidly in the shaft to allow tool deployment and drilling of the blocking stones.
5. The robot must be capable of carrying and deploying a drill of minimum length 360 mm as calculated from the thickness of the first blocking stone (60 mm), plus the estimated blocking stone chamber length (200 mm), plus a second blocking stone of maximum thickness 100 mm. A drill diameter of 28 mm was chosen to be the smallest that can be used to open up the previous hole size of 1 in. and allow access to the second blocking stone.
6. The robot must be capable of climbing at a 40° angle against gravity for 70 m while pulling its tether, and carrying tools and cameras of a maximum weight of 600 g. The maximum tool weight is an estimate from the predicted drill weight.

7. The robot must be capable of climbing over a 40 mm step while climbing against gravity and pulling its tether. The step occurs at an approximate distance of 59 m within the shaft.

This paper details robots developed and deployed within the southern shaft of the Great Pyramid. Section 2 examines the literature around climbing robots for similar applications. Section 3 develops the theory of climbing steps and generating traction to overcome the step. Section 4 describes the development of several prototypes to investigate solutions. Section 5 details the design of the final robot configuration, including the design of a snake arm camera and a long reach drill. Section 6 presents the results of lab-based experimental trials to evaluate the step-climbing and drilling performance.

Section 7 describes a deployment inside the Great Pyramid, and it will show that the robot performed exceptionally well and reached the top of the southern shaft after traveling 63.6 m while protecting the pyramid from damage through an inchworm locomotion system. A bore scope was deployed through the blocking stone and viewed almost the full interior of the chamber for the first time. Many interesting and useful shaft features were observed that will help to fulfill the primary objective of the mission, including writing that has been hidden for thousands of years. Finally, Section 8 draws conclusions from the work.

2. CLIMBING ROBOTS

Pipe inspection robots are the closest commonly researched analogy to the problem of exploring shafts. Robots designed to inspect pipelines must exhibit flexibility to adapt to the changing shape, size, and configurations of the pipelines. This requires the robots to possess active steering capability and also sufficient traction to pull the tether cable, climb vertical pipelines, and surmount obstacles (Choi and Ryew, 2002). Pipe inspection robots can be classified at a basic level around their movement patterns: (i) wheeled reaction;

wheels are sprung to oppose each other to create a high normal force for traction, (ii) track reaction; tracks are sprung opposite to each; and (iii) inchworm; a robot sequentially applies, removes, and moves opposing reaction force sections (Roh and Choi, 2005).

The majority of pipe inspection robots use passive spring-linkage mechanisms (Fujiwara et al., 1994; Okada and Kanade, 1987; Taguchi and Kawarazaki, 1997) to create large normal forces for their drive wheels. However, few of these robots can successfully navigate complicated configurations such as inclines, elbows, or "step" changes in a cross-sectional area. A robot that uses an extension spring, connected to the wheel limbs to provide the robot with enough clasping force, is shown to climb cables on a cable-stayed bridge during inspection (Xu and Wang, 2008). The robot relies on the driving torque of the motor and requires a safety system in case of electronic failure to prevent falling. Similar use of wheels mounted on spring damper limbs has been demonstrated to ensure a known traction force (Huang et al., 2010; Lu et al., 2007). A variation of this is achieved using high-grip caterpillar tracks driven by dc motors combined with mechanical linkages to regulate normal force based on the pipe diameter (Kim et al., 2009). A force feedback loop ensures consistent traction against the walls. A design modification to such systems uses magnetic wheels (Kawaguchi et al., 1995) for climbing obstructions and overcoming bumps, but it is limited to passages composed of magnetic materials. Additionally, many of these systems do not demonstrate an active steering capability which allows them to selectively navigate branches in the pipeline. A robotic system with active steering capability for inspection of urban gas pipelines was presented in Choi and Ryew (2002). The system consists of two active driving modules at the front and rear of the system with optional passive modules linked in between them. A steering mechanism with compliance control called the Double Active Universal Joint (DAUJ) prevents rolling of the robot along its driving direction. However, the complexity of the mechanism only allows space for small wheels that are not suitable for climbing steps in pipes. Furthermore, the mechanical actions of the reaction wheels severely impede step climbing.

Previous robots have been designed to operate in circular pipes. The family of Explorer robots (Schempf et al., 2010) is one such example. The robot is modular in nature, with sizes of the segments driven by several factors including obstacle navigation, pressure drops, and packaging minimization. Locomotion is achieved via traction-based propulsion, where contact forces generate friction to allow pipe internal driving. Articulated arms allow the robot to drive at the bottom or center itself within the pipe. This is very similar to some of the prototype designs of the Djedi robot (with both passively and active sprung modules) described in Section 4. Robots designed to climb in square shafts have the advantage that the parallel wall faces can

provide a restoring force to prevent robot rotation around the axis of the shaft; however, they have the disadvantage that the diagonals are longer than the horizontal and vertical distances, and therefore they are more likely to lose traction if rotation occurs.

Overall, the sprung reaction method of climbing tunnels has several key disadvantages for the problem here:

- The reaction forces are difficult to control, resulting in problems traversing steps and other obstacles in the shaft.
- The complexity of the mechanism only allows room for small wheels that are incapable of traversing obstacles.
- The rolling contact under the reaction forces results in wheel slip and probable damage to the tunnel surface.
- The sprung compliance of the wall contact results in a lack of rigidity that can degrade the performance of cameras and make the deployment of tools difficult.

Mechanisms can be used to create passive suspensions that increase vehicle traction and step-climbing ability (Thueer et al., 2006). An example of this type of system is the Rocker-bogie configuration deployed on the Mars robotic expedition. Using this technique, it is possible to climb steps the size of the wheel radius. However, these mechanisms require considerable volume and are not suitable for deploying in confined spaces.

An alternative approach would be to develop a legged robot for the task. Many varieties of legged robots have been shown to successfully climb stairs including, hexapods (Moore and Buehler, 2001; Saranli et al., 2001), quadrupeds (Buehler et al., 1998; Hirose et al., 1994; Talebi et al., 2000), and bipeds such as the Honda humanoid robot (Hirai et al., 1998). However, researchers have been unable to successfully develop legged robots to climb in confined spaces such as pipes. Moreover, developing a legged robot with the primary aim of climbing a single step is hugely inefficient in terms of complexity and weight. In addition, controlling the legs accurately at large distances from human operators in a loosely defined environment is risky.

Inchworm robots could be considered to be a simplified variant of a legged robot. Inchworm robots grip with one section of the robot and move with another, thereby preventing moving contact at the attachment point. Inchworm robots are frequently used to locomote in passages such as pipes. The robots generally have a front and rear section, each with a method of gripping the walls of the pipe or shaft; these are typically pneumatic (Lim et al., 2007; Yoon and Park, 2010) or solenoid-driven (Shin et al., 2010). The working principle involves the rear module gripping the sides of the wall while the front releases. The front module then moves forward and grips. Finally, the rear module releases and moves forward, completing the cycle. Bends are negotiated by allowing the robot to pivot in the middle, allowing the front module to follow the contours of the

passage (Bertetto and Ruggiu, 2001; Choi et al., 2010; Fukuda et al., 1987; Lim et al., 2007; Shin et al., 2010). An extension to a conventional inchworm robot is a combination of two inchworm systems (one for longitudinal the other for rotation). This type of robot overcomes rotation in the axis of the pipe, which is problematic, at the cost of increased complexity (Yoon and Park, 2010). Inchworm systems provide a stable base due to reaction forces exerted without a compliant element. However, during inchworm motion, one section of the robot needs sufficient traction to support the end that is free to move. Moreover, the sequence of steps for locomotion requires computer control and is slower than wheel locomotion.

3. ROBOT THEORY

Climbing the shafts presents two big challenges: (i) Generating sufficient traction to overcome gravity and friction of the robot and umbilical, and (ii) climbing a step while maintaining climbing traction. These two challenges are not independent, and methods of increasing traction on inclined shafts are likely to significantly degrade step-climbing capability.
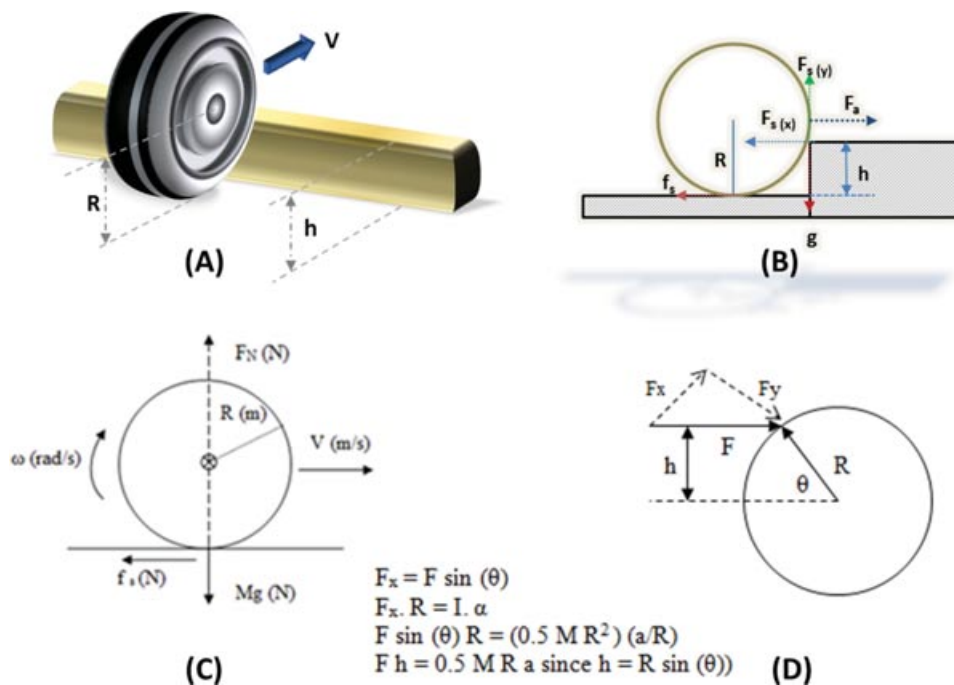
3.1. Analysis of Wheel Rolling Motion

The diameter of a wheel determines the forces required to roll it over a step. Consider the scenario of Figure 4(A). A wheel of radius R is rolling toward a step of height h. It is desirable to minimize the forces required to traverse a step while minimizing the radius to make the robot as compact as possible. Figure 4(B) shows a free body diagram in the wheel and step scenario, where g is the force due to gravity. $F_s(x)$, $F_s(y)$, and F_a are the horizontal component of the reactive force, the vertical component of the reactive force (due to the wheel rolling forwards), and the force that drives the wheel forward, respectively. f_s is the static friction contact where the wheel makes contact with the ground and R is the radius of the wheel. To drive over the step, the sum of the forces must result in a positive value of $F_s(y)$.

If the angular velocity ω of a rotating object is such that $R.\omega$ is the same as the linear velocity V of the center of mass, and F_n is the normal force due to gravity [Figure 4(C)], the object is assumed to be rolling without any slippage [Figure 4(C)]. The static friction f_s causes the rolling of the mass M_r due to the torque τ generated, i.e.,

$$\tau = f_s.R = I\alpha, \tag{1}$$

where I is the inertia of the mass $(0.5M_r R^2)$ and α is the angular acceleration of the mass. For rolling without slipping to occur on the application of a force, it can be shown that the force has to act at a height $0.5R$ above the center of the mass [as derived in Figure 4(D)], where θ is the angle subtended between the point of application of the force and parallel to the ground, as shown. Minimizing slippage is important as slippage is a loss of energy resulting in the requirement of higher forces to climb steps.

$$F_x = F \sin(\theta)$$
$$F_x.R = I.\alpha$$
$$F \sin(\theta) R = (0.5 M R^2)(a/R)$$
$$F h = 0.5 M R a \text{ since } h = R \sin(\theta))$$

Figure 4. Free body diagrams to analyze wheel rolling motion. (A) Perspective view, (B) step climbing free body diagram, (C) rolling without slipping, (D) relation between radius of wheel and height of application of force above the wheel center.

3.1.1. Locomotion Over a Step

For a wheel of radius R to be able to climb a step of height h, the vertical component of the force exerted by the step $F_{s(y)}$ upon the wheel must counteract gravity g, so that it lifts off the ground. Note that $F_{s(y)}$ includes any frictional forces between the material of the wheel and the step. If F_a is the horizontal component of force that drives the wheel forward, $F_{s(x)}$ is the horizontal component of the reactive force from the step, and f_s is the (static) frictional force where the wheel makes contact with the ground, it can be shown that the following condition must be satisfied to enable the wheel to climb the step:

$$F_s(x) > \frac{M_r.g\sqrt{R^2 - (R - h)^2}}{(R - h)} + f_s. \qquad (2)$$

Note that if R is equal to h, no amount of force will be sufficient to ensure that the wheel climbs the step. It follows that the greater the radius of the wheel with respect to the height of the step, the lower the force required in achieving the same torque, and correspondingly the lower the effort in climbing the step.

By using the step-height data from that inside the tunnel, i.e., step height = 40 mm, a normalized plot of the force required to climb the step for different wheel radii is shown (Figure 5). The decaying nature of the relationship shows that using a wheel of larger radius beyond a certain value does not offer any significant advantage, as seen in Figure 5. By analyzing the theory behind rolling without slipping and the locomotion over a step, it follows that a good choice for the diameter of the wheel chosen during the design should be three times the step height, so that the point of contact of the step with the wheel occurs at 0.5 times the radius above the center of the wheel. If slipping occurs during the climb,
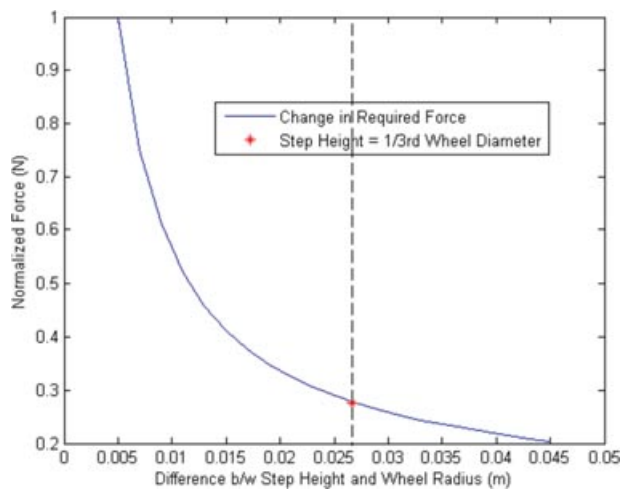
Figure 5. Effect of change in wheel diameter vs. constant step height.

the effective torque on the wheel is reduced, resulting in an increased energy expenditure.

In actuality, there are different dynamics for a front wheel climbing a step compared to a rear wheel. If pushing and pulling occur along the same parallel axis, there is no difference in effort. When the rear wheel is pulled over the step, the front wheel has already climbed the step and has increased the angle and hence the vertical component of force. Therefore, the rear wheel can be smaller than the front wheel while the same forces are exerted.

3.2. Climbing Ideal Slopes

To climb an incline, a robot of mass M_r on an incline of θ_a must generate sufficient pulling force F_p to overcome gravitational force F_g, frictional drag forces F_d, and the forces require to drag the tether (F_c).

The gravitational force can be resolved into a component of force along the shaft and normal to the shaft wall [Figure 6(A)]. The following equations are valid for the free body diagram:

$$F_r = M_r.g.\sin(\theta_a), \qquad (3)$$

$$F_g = M_r.g.\cos(\theta_a). \qquad (4)$$

The pulling force that the robot can exert (F_p) is limited by the friction coefficient between the robot and the shaft surface (μ_n) and the normal force (F_r),

$$F_p \leq F_r.\mu_n. \qquad (5)$$

To overcome the umbilical force, the forces due to the cable, gravity, and friction need to be overcome. If (μ_c) is the friction coefficient between the cable and shaft, C_m is the cable weight per meter, and x_c is the distance climbed in meters, then the force required to pull the cable can be found:

$$F_c = C_m.x_c.\mu_c + \mu_c.x_c.\cos(\theta_a). \qquad (6)$$

Therefore, in order to climb the shaft, the required pulling force is

$$F_p = F_g + F_c = M_r.g.\cos(\theta_a) + \mu_c.x_c[C_m + \cos(\theta_a)]. \qquad (7)$$

Maximising the friction coefficient between the wall and robot is the most straightforward method of climbing the steepest slope. It is possible to use sticky tyres to increase this coefficient beyond that of normal material, however it is likely that this will leave residual material and the tyres will soon lose stickiness in the presence of dust and grit.

3.2.1. Using Opposing Reaction Forces on Ideal Tunnels

If the robot is climbing within an enclosed space, then the reaction force F_r can be augmented by applying opposite force F_O on a surface parallel to the drive surface, resulting
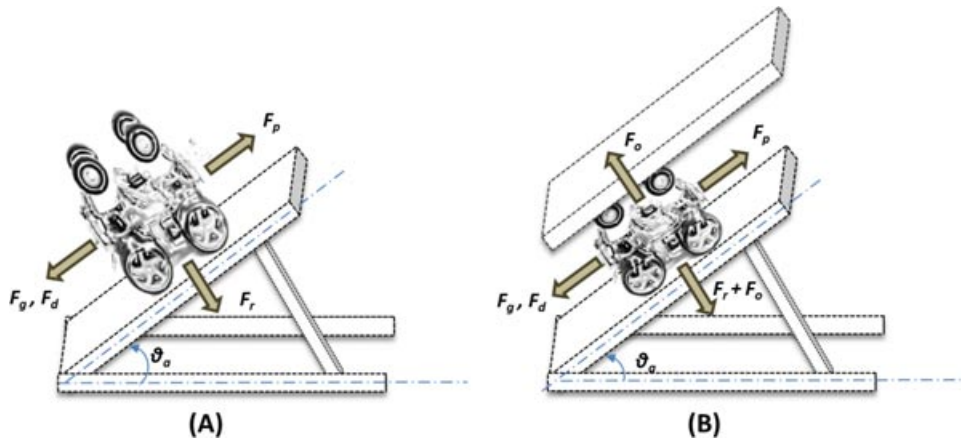
Figure 6. Free body diagrams of climbing robots. (A) Open incline, (B) enclosed incline.

in an increase in the maximum pulling force that can be applied [(Figure 6(B)].

$$F_p <= (F_r + F_o).\mu_n \qquad (8)$$

For a shaft and step climbing robot there is a complex relationship between the required opposing force, traction force and vehicle mass. For example, a larger opposing force will require more drive traction to climb the step, and this in turn will require larger motors requiring more opposing force (a vicious circle). A successful robot design using opposing force should seek to minimize the vehicle mass, thereby requiring smaller motors, less opposing force, and less drive traction (a virtuous circle). Equation (2) can be modified to include the effect of opposing force for step climbing on an incline at an angle θ, within an enclosed space,

$$F_s(x) > \frac{[M_r.g.\sin(\theta) + F_O]\sqrt{(R^2 - (R - h)^2}}{(R - h)} + f_s. \qquad (9)$$

It is clear that the component F_O directly affects the climbing performance.

4. CONCEPTUAL DESIGN ITERATIONS: VARIOUS CONFIGURATIONS OF THE DJEDI PROTOTYPES

The vehicle design philosophy was to minimize the vehicle mass, cable drag, and therefore stress on the shaft walls. Toward this goal, the aim was to create the simplest robot (therefore the lightest, minimizing the required traction forces) and ensure that the contact between the robot and shaft wall was through soft compliant material. Initial evaluation of the design requirements resulted in the conclusion that an approach based around soft rubber wheels could provide the correct amount of traction while retaining a simple and reliable design requiring little onboard electronics. To understand the complex robot dynamics, several

mechanism prototypes were constructed and tested in a lab-based test environment.

Prototype 1 [Figures 7(A) and 7(B)]: This robot featured eight independently sprung arms supporting seven driven wheels and one pair of passive stabilizing wheels. Each sprung wheel could be retracted from the wall through a motor and tendon arrangement mounted on the robot; seven drive motors and eight motors to retract the sprung arms from the wall. The prototype rover was constructed from fiber-reinforced plastic chassis, carbon fiber rod, and rubber wheels with aluminum centers and is essentially a skeleton of the finished overall expedition robot. The suspensions can deform to traverse obstacles while maintaining traction. The robot was prone to roll around the axis of the shaft due to a single wheel contact on each face of the square shaft and was therefore discounted from this work. However, the robot configuration would be well suited for climbing in circular shafts.

Prototype 2 [Figures 7(C) and 7(D)]: The second prototype was created from four large independently driven ground wheels combined with four actively sprung, passively driven wheels under tension against the top of the shaft. The tension was implemented through a series elastic actuator that allowed reduction in normal force at each wheel for tasks such as step-climbing. The wheels were steered thorough a differential steering action, where uneven torque applied to wheels of a drive pair caused the wheel axis to twist around a central rotation point. Control of the wheel torque enabled accurate steering, for example (i) the front wheels apply different torques, causing the wheel axis to twist with respect to the vehicle body; (ii) opposing differential torque stops the axis from twisting; and (iii) when the wheel torque is even, the wheel axis does not rotate and the robot drives in the direction of the wheel pair. PID control was applied to each pair of drive wheels, resulting in four-wheel steering. The prototype was
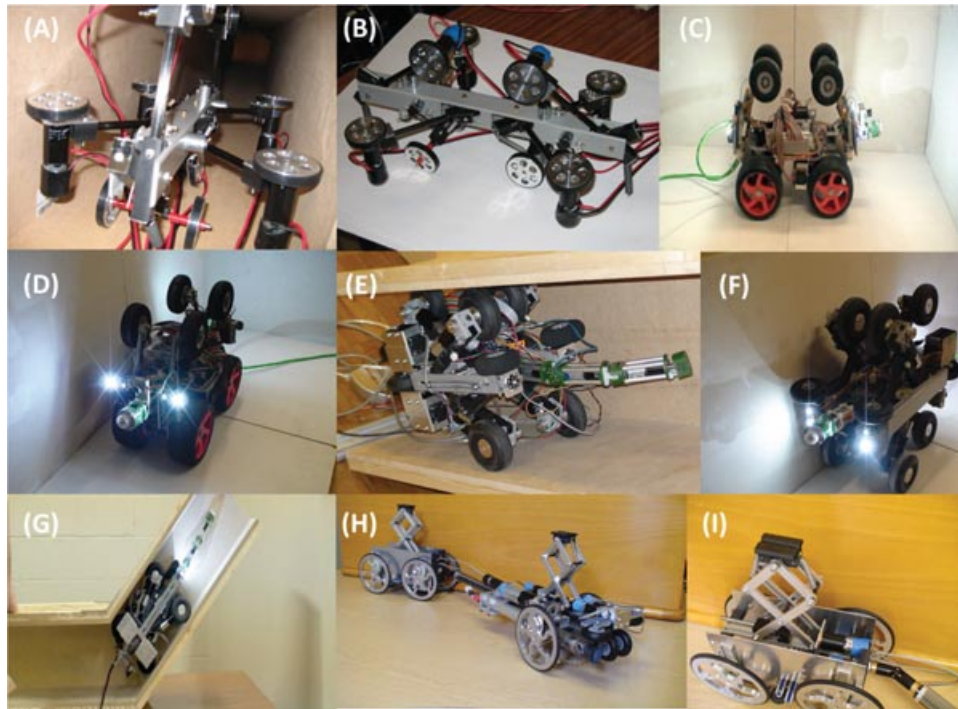
Figure 7. Prototype Djedi designs: (A) and (B) show Prototype 1 with eight independently sprung arms. (C) and (D) show Prototype 2, which featured four actively sprung, passively driven wheels. (E), (F), and (G) show Prototype 3 with six independently driven wheels combined through a mechanical linkage arrangement. (H) and (I) show the inchworm-based robot concept in development.

manoeuverable and capable of climbing a shaft; however, driven wheels on one shaft face significantly reduced robot traction and the robot was not successful at climbing a step.

Prototype 3 [Figures 7(E), 7(F), and 7(G)]: The third prototype was designed to create a more uniform normal force on two faces of the shaft. Six independently driven wheels (three opposing pairs of wheels) were combined through a mechanical linkage arrangement. The mechanical linkage was carefully designed to minimize variation of normal force as the shaft size varies. Furthermore, extension of one wheel resulted in extension of the opposing wheel, thereby keeping the robot body central in the shaft. The robot performed well in the shafts, providing traction over variations in shaft height and through the entrance transition from horizontal to vertical. However, it suffered from poor step-climbing ability and was only able to climb over a 20 mm high step.

Conclusions on wheel-based prototypes: Following the testing of prototypes 1 to 3, it became clear that the requirements of high traction, soft wheels, traversing the step, and entrance transition from horizontal to vertical were not feasible; a tradeoff between opposing force and traction could not be achieved. Furthermore, the drilling technology had been developed in parallel and it was clear that the drill

would be relatively heavy, long, and require a stable base. Therefore, a prototype based around inchworm technology was created; this approach had previously been discounted due to the complexity of design and its requirement for more complex onboard electronics. An inchworm robot eliminates the tradeoff between an opposing force and step-climbing ability, as these no longer conflict.

Djedi prototype [Figures 7(H) and 7(I)]: A prototype inchworm-based robot was created. An active jack was mounted on a rack and pinion carriage, allowing forward and backward inchworm motion along the shaft. A drill was mounted on another carriage and driven by a rack and pinion system on the same rack as the linear jack. A second active jack was mounted on a body section joined to the first body section via a universal joint. Passive wheels were used to prevent the body dragging during the motion. The front and rear body sections contained sideways pushers to move the body section left and right in the shaft. The robot worked exceptionally well. It was able to climb the shaft, traverse the step, and provide a very stable platform for drilling.

Refinements for the final design: The inchworm design was selected to be taken forward for full development, taking into consideration several lessons learned:
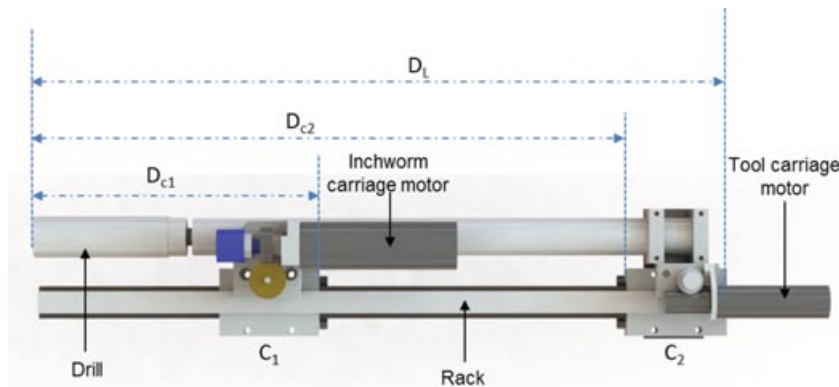
Figure 8. The rack with mounted carriages, motors, and drill illustrating the maximum tool deployment (Dc2 - Dc1).

- The pushers and jacks of the inchworm prototype were bulky and heavy, bracing on the shaft walls both vertically and horizontally. A more elegant solution was to replace these with compact linear actuators based around Firgelli miniature actuators. These actuators are compact and consist of a lead screw combined with a sheet potentiometer, all in a cylindrical case. Their compactness enabled them to be mounted horizontally on the robot (no vertical bracing) and to be used for steering as well as bracing; bracing vertically is not a requirement for climbing, as sufficient traction can be generated from the sidewalls alone.

- Articulation between the two body sections was not required, as steps could be climbed with a rigid articulation section due to compliance in robot structure and braces.

- Metal bodywork made the robot heavy and alternative materials should be used for the bodywork and other nonessential parts.

5. DETAILED DESIGN AND DESCRIPTION OF DJEDI

The Djedi robot was based around the prototype robot, consisting of two pinion carriages mounted on a single rack and driven independently by motors and gears. The first carriage implements the forward and backward inchworm motion from a Maxon Amax32 with a gear ratio of 66:1 and transmitted to the rack pinion through cross-helical gears, resulting in a maximum transmissible rack force of 843 N. The second carriage implements tool movement for deployment of the drill or snake camera and is driven via a Maxon Amax22 motor with a 370:1 gearbox combined with a worm gear ratio of 20:1. Therefore, it has a total gear ratio of 7400:1. The maximum torque output is approximately 2500 N, with failure due to worm gears or rack/pinion limiting the force output. This level of force is not required with the main requirement for low speed (min 0.1 mm/s, max 0.63 mm/s) and non-back-drivable motion in the presence of drill loads

(i.e., uniform drill speed regardless of load). There is a design tradeoff between the robot successfully manoeuvering through the shaft and the maximum length of tool deployment. Figure 8 illustrates the rack: two carriages (C_1 and C_2) with motors and drill. Note that the motor and bracket of carriage 1 sit above the drill, allowing independent movement of carriages 1 and 2.

The maximum tool deployment (drill depth) is the distance D_{c2} from the front of the robot to the front of the tool carriage C_2 minus the distance D_{c1} from the front of the robot to the back of the inchworm carriage C_1. The length D_{c1} should be minimized, but in reality some space is needed to accommodate components such as wheels, braces, cameras, and lights. The overall length of the rack D_L needs to be maximized to allow the longest tool deployment while still passing through the shaft and in particular the initial transition from horizontal to 40°. The length of components overhanging the rack needs to be minimized to maximize the rack/robot length ratio. Components such as the carriage 2 motor unavoidably protrude beyond the rack.

The inchworm motion alone would cause the robot base to be dragged along the shaft floor, resulting in high friction, likely damage to the shaft, and it would be incapable of traversing a step. Therefore, four free-to-rotate wheels are included on the robot, two at the front and two at the rear. Importantly, these wheels are not powered; their only function is to prevent dragging along the floor and allow steps to be climbed. The front wheels were 126 mm diameter and the rear wheels were 90 mm diameter; the smaller rear wheels resulted in a more compact rear section while still allowing step climbing as they will be pulled over the step requiring less force. Custom-built actuators were developed to apply bracing force to the wall. These actuators consist of a small geared motor and lead screw arrangement producing a force output of 50 N and 100 mm length of travel. A silicone rubber brace pad cast with an inbuilt flexi-force force sensor was mounted on the end of each brace actuator. The resolution of the flexi-force sensor was limited; however, it was adequate to provide
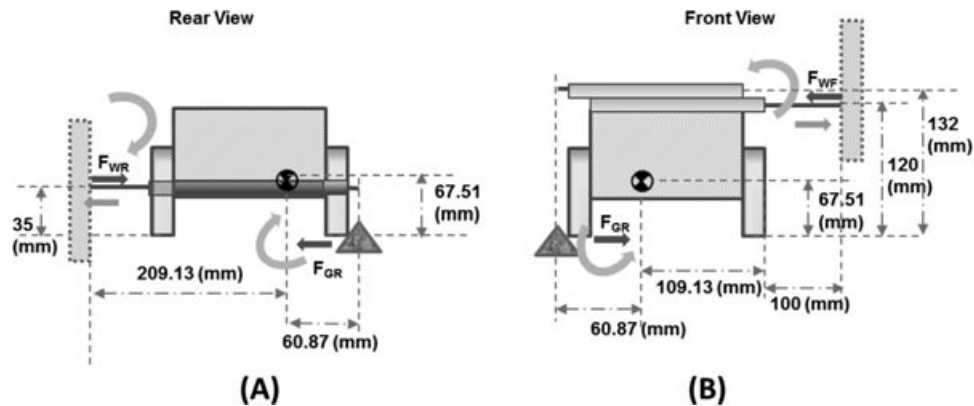
Figure 9. Effect of bracing on robot moments. (A) View from the rear of the robot, (B) view from the front of the robot.

three reliable force readings: no force, medium force, and high force. When the braces are actuated, the wheels slide along the floor. However, the sideways motion may be restricted by surface roughness of the shaft and generate a moment around the robot. The robot was designed with the front braces positioned high on the robot and the rear braces low on the robot. Figure 9 illustrates the scenario of the wheel's sliding motion restricted by bumps on the shaft floor; Figure 9(A) shows the front of the robot and Figure 9(B) shows the rear of the robot. The torques generated as a result of the robot bracing can be computed as below (where 132 and 35 are the height in mm of the center of the brace from the shaft floor):

$$T_f = (0.132)F_{WF} \tag{10}$$

$$T_r = (0.035)F_{WR} \tag{11}$$

Therefore, the front (high) braces are capable of producing more than three times the moment of the rear actuators. The front brace actuators are positioned on top of each other, resulting in slightly different moments depending upon which one is actuated. Therefore, the exact ratio between the maximum moment of the front braces compared to the rear braces is

$$T_f = 3.77T_r \text{ (for the right braces)},$$
$$T_f = 3.428T_r \text{ (for the left braces).} \tag{12}$$

This ratio may be a sufficient moment to overcome the frictional forces of the rear bracing within the tunnel walls, which could cause the robot to "roll" inside the tunnel.

Ideally, the height of the brace actuators would be as low as possible to minimize unwanted roll as a result of restricted wheel motion during bracing. However, at the front of the rover, this would result in brace actuators clashing with tool movement or lengthening the front of the robot to reduce tool deployment length. Furthermore, it is important that the front wheels are in line with the front of the
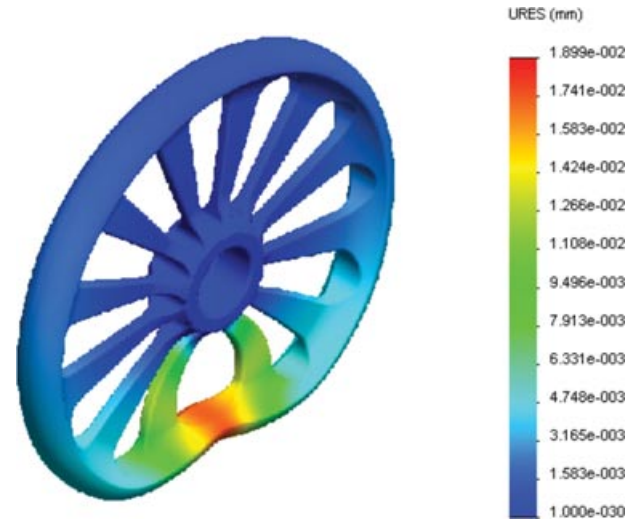

Figure 10. Wheel deflection for 100 N vertical load (wheel diameter: 126 mm; wheel thickness: 10 mm).

robot for step climbing, and the relatively large radius of the front wheel further prevents low positioning of brace actuators. Therefore, as a design tradeoff the front braces were positioned high on the robot and the rear braces were positioned low down.

The bodywork of the robot was designed to minimize mass and provide the strength to mount the brace actuators and house the electronics and cameras. The 3D CAD models were directly reproduced using a laser-sintering process. This manufacturing process is ideally suited for generating quick prototypes, but it also has sufficient strength for functional components. For example, Figure 10 illustrates an analysis performed to predict the deflection of a rapid prototyped front wheel under a 100 N vertical load. The maximum deflection is 0.02 mm and will not affect the wheel rotation.
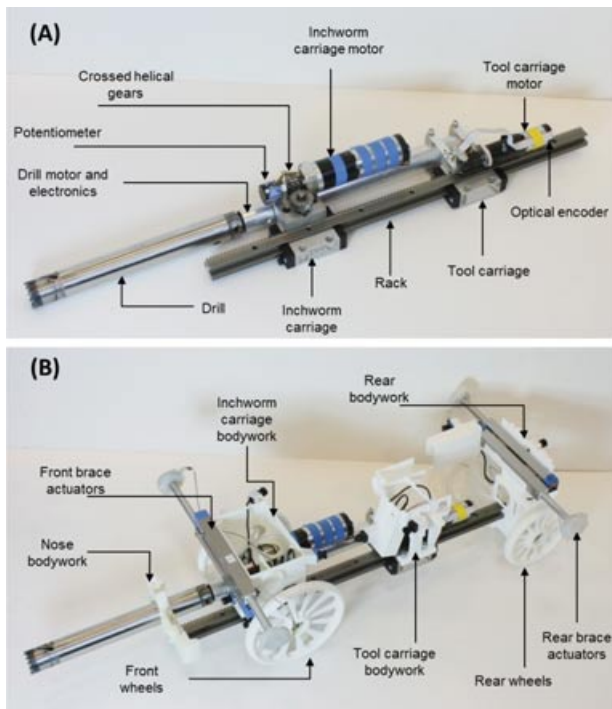
Figure 11. (A) The rack and carriages; (B) the brace actuators, wheels, and main bodywork sections.

Figure 11 illustrates the robot chassis and key components during assembly. Figure 11(a) illustrates the rack, carriage, and motor arrangement; note the drill is positioned underneath the inchworm carriage motor. Figure 11(b) illustrates the addition of carriage bodywork, brace actuators, and wheels. Figure 12 illustrates the full robot with sensors and peripheral components, and Figure 13 illustrates the final robot being deployed into the shaft. The weight distribution of the robot is presented in Table II. Almost half of the weight of the robot is from the rack, motor, and carriages. The drill was the heaviest tool, weighing in at nearly 600 g.

5.1. Command, Control, and Electronics

The design philosophy for the Djedi control system was to minimize the risk of robot failure within the shaft through not relying on the onboard electronics or embedded control software to perform a task that could result in the robot falling within the shaft. As an example, if the onboard controller incorrectly sequenced the bracing actions, a scenario could occur in which all braces were removed from the shaft. Therefore, a control strategy was formulated in which the onboard electronics perform closed-loop feedback on lower-level systems, such as brace actuator positions and carriage positions. The sequence of higher-level commands (i.e., brace front actuators and release rear actuators) was

commanded from a laptop PC. Therefore, the instant the PC is commanded to stop a movement sequence, no further higher-level commands will be sent to the robot. The downside to this strategy is a delay in robot response following a command from the laptop computer.

5.1.1. Communication and Umbilical

Data communications were implemented through RS485, which allows several devices to communicate at half-duplex on a single pair of wires, plus a ground wire at distances up to 1200 m. Onboard the rover, there were three control boards positioned in different robot sections and daisy-chained together. The serial protocol directs commands to the appropriate board. Each robot control board contained multiple servo outputs, H-bridge voltage outputs, and sensor inputs. Composite video was fed through video switchers on each robot section. Each video switcher was capable of switching 10 cameras. The base camera switcher also switches between the other camera switchers (losing 2 cameras); 28 miniature cameras can therefore be viewed on the robot (1 camera at any one time). A video balun was used to convert composite video to be transmitted over the length of the tether with minimal losses. Power converters on robot sections converted 60 V down to 12 V for powering electronics, cameras, and motors. The actuators were position-controlled through onboard PID control loop hardware.

The inchworm carriage and tool carriage move with respect to the rear chassis of the robot. Electrical power and communications are passed between the base and the carriages through a recoiling cable arrangement that consists of a spiral torsion spring and cable reel; as the carriages move, extra cable is uncoiled to maintain electrical connection.

The umbilical between the robot and base contained six wires in a custom-made lightweight sheath with a weight of 24 g/m. Lines 1 and 6 supplied power to the robot at 60 V, lines 2 and 3 were for data communication, and lines 4 and 5 were for video. Copper was chosen over fiber optic for data and video transmission due to the size and weight of the available video and data converters required onboard the robot; it is also a significantly cheaper option with adequate performance. Transmitting power through a high-voltage converter allows thinner wire and has a significant impact on the umbilical weight.

5.1.2. Sensors

Sensors onboard the robot provide invaluable information on the robot's internal and external environment. These parameters are detailed in Table III. The primary sensors were the brace actuator position and inchworm carriage position sensor. The pitch, roll, and tilt sensor was primarily used to measure the shaft orientation.
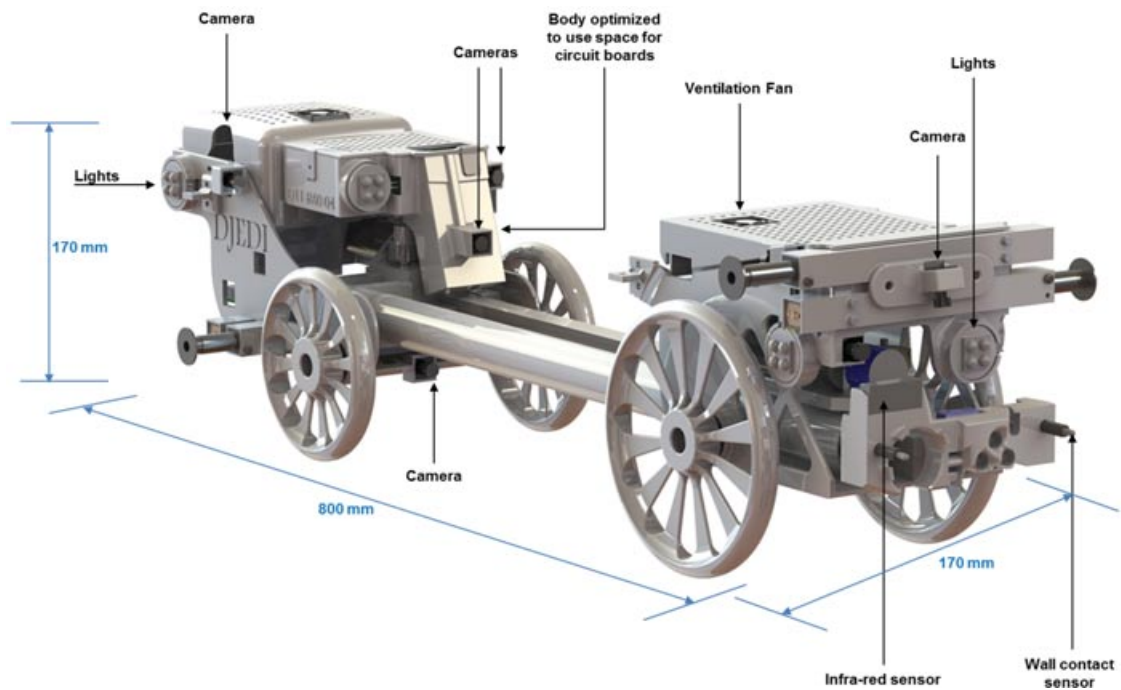
Figure 12. Rover sensor and peripheral detail.

Figure 13. The Djedi robot being deployed in the shaft of the Great Pyramid (Photo: Sandro Vannini).

5.1.3. Controller Implementation

To climb the shaft, sequential commands were automatically generated from the laptop to perform forward or backward locomotion. A graphical user interface (Figure 14, inset) allowed an operator to adjust the robot's stride length and its center position, i.e., the robot could take full steps, small steps with the front carriage at the front or rear, or any combination in between. The user was also able to alter the minimum and maximum extension of the brace pads. This allowed the user to alter the robot's lateral position within the tunnel, so it could drive closer to the left or right side of the wall. More importantly, it allowed the user to control the robot when driving through a lateral step. In should be noted that in this scenario, the center position of the front

Table II. The components of the robot and their weights.

Component(s)	Weight (Kg)
Rack (650 mm long), carriages, carriage motors	1.284
Bodywork, circuit boards, lights, brace actuators, wheels, cameras	1.528
Weight, no tools	**2.812**
Snake camera	0.128
Drill (including motor, mounting bracket, and corer)	0.574
Maximum weight (robot and drill)	**3.386**

and rear braces will be different. The laptop displayed real time feedback of all robot systems including brace positions. Figure 14 illustrates the control system set up in the queen's chamber of the Great Pyramid.

Video was displayed to the user though a separate video monitor. The user could also take direct control of any actuator including the brace actuators and rack motors, although this was forbidden during climbing to minimize risk of the robot falling.

5.2. Inchworm Locomotion

A sequence of bracing, and unbracing, and altering the inchworm carriage position results in forward or reverse motion. Figure 15 illustrates the robot sequence for a reverse motion. Initially, the robot has all braces against the shaft [Figure 15(A)]. In Figure 15(B), the front braces are released. The inchworm carriage moves toward the back of the robot next [Figure 15(C)]. In Figure 15(D), the front and rear actuators are braced. Finally, the inchworm carriage moves toward the front of the robot, resulting in backward movement of the rear of the robot. The sequence then repeats.

The number of operations required for an inchworm step results in a relatively slow locomotion method, with the time taken to perform each stage and the step length being crucial factors. Assuming the robot is in the center of the tunnel (i.e., left and right braces take the same time to reach the tunnel wall), the time for each sequence can be calculated. The time for each step (T_s) is a function of the brace velocity (B_{vel}), the length of brace travel (B_{dist}), the rack velocity (R_{vel}), and the rack distance (R_{dist}). During a full sequence each pair of brace actuators is required to unbrace and brace; therefore, the time for four brace operations is required. The inchworm carriage moves from the front to the back and then returns, requiring the time for two operations. A factor of 1.2 has been included to allow for any variation in motion; without this factor, subtle variations in obtaining a good brace could result in the robot falling.

Therefore, the time taken for each step is

$$T_s = 1.2 \left(4 \frac{B_{dist}}{B_{vel}} + 2 \frac{R_{dist}}{R_{vel}} \right). \qquad (13)$$

The total distance traveled during this motion is R_{dist} (one inchworm carriage motion), therefore the climb velocity (C_{vel}) can be found from

$$C_{vel} = \frac{R_{dist}}{T_s}. \qquad (14)$$

Combining Eq. (13) and (14),

$$1.2 \left(4 \frac{B_{dist}}{B_{vel}} + 2 \frac{R_{dist}}{R_{vel}} \right) = \frac{R_{dist}}{C_{vel}}. \qquad (15)$$

Rearranging,

$$C_{vel} = \frac{1}{1.2} \left(\frac{R_{dist} B_{vel}}{4 B_{dist}} + \frac{R_{vel}}{2} \right). \qquad (16)$$

The velocities of the rack, braces, and distances they travel determine the climbing velocity. The velocities
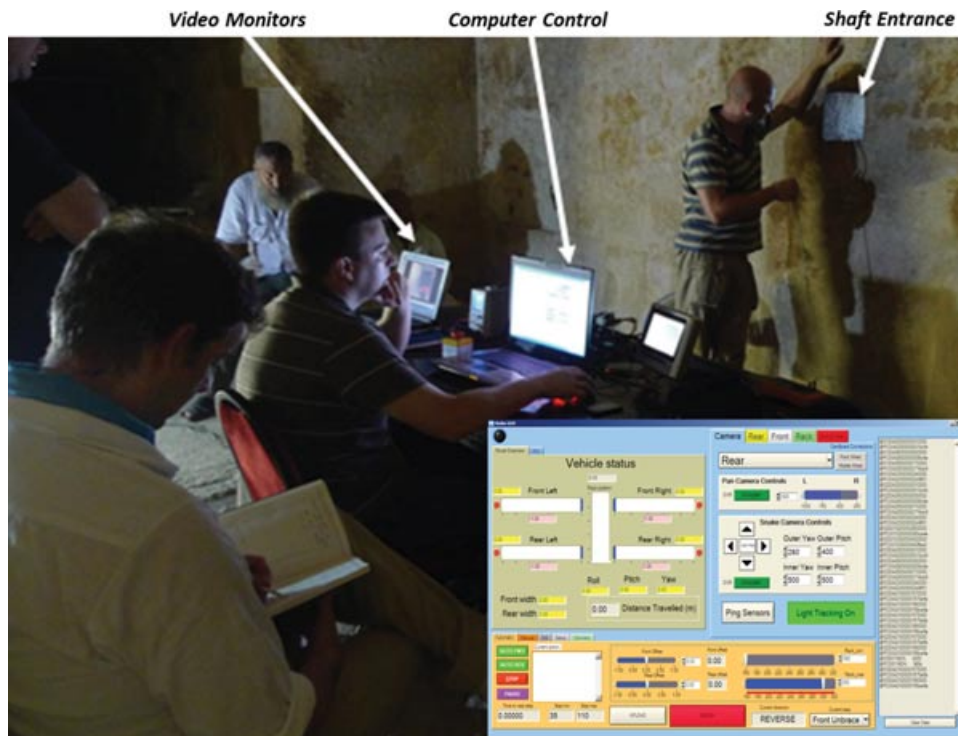
Table III. Sensors onboard the robot.

Sensor	Number of inputs	Purpose
PSU temperature	x 3	Monitor temperature of power conversion electronics
Pad force	x 4	Monitor contact of brace actuators
Actuator position	x 6	Measure the position of brace actuators, carriage position on the rack, and tool position on the rack
Drill motor temperature	x 1	Monitor the temperature within the drill power converter and motor
Nose contact	x 1	Monitor for contact of the rover nose
External air pressure sensor (altitude)	x 1	Measure air pressure around the robot to assist in altitude calculations (prone to errors due to ambient heat)
Pitch, roll, and tilt	x 3	Measure the rover orientation in the shaft
IR proximity sensor	x 1	Monitor the distance from the robot nose to the blocking stone
Actuator current	x 5	Monitor the current draw of the actuators

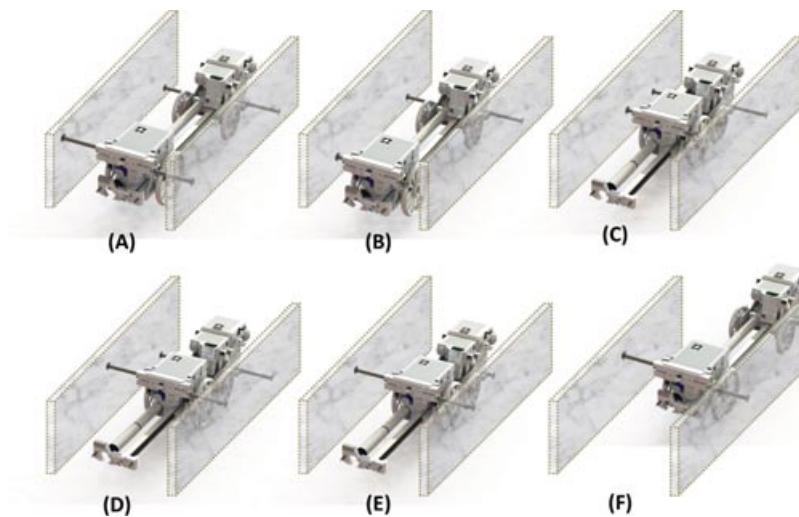**Figure 14.** Command control and the graphical user interface.

Figure 15. Renders of various possible configurations of the Djedi robot during inchworm locomotion. (A) All pads braced. (B) Front pads retracted. (C) Body decreased in length. (D) Front pads braced. (E) Rear pads retracted. (F) Body increased in length.

are determined by the motors and gear ratios. It is not a straightforward task to alter these, as higher velocities requires larger and heavier motors, which in turn impact upon the forces required to climb the shaft.

Therefore, it is crucial that the ratio R_{dist}/B_{dist} is maximized; the largest possible rack length should be selected and the braces should travel the smallest possible distance.
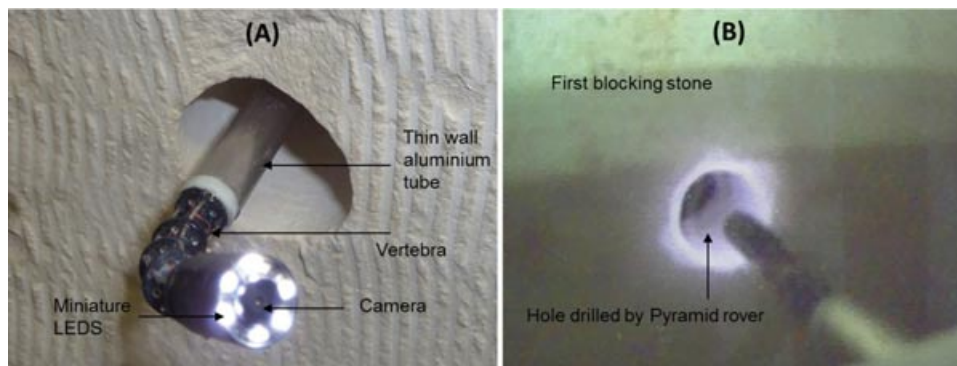
Figure 17. The Tendon Arm camera under test: (A) Deployment in a lab-based environment. (B) Deployment through the first blocking stone of the queen's chamber.
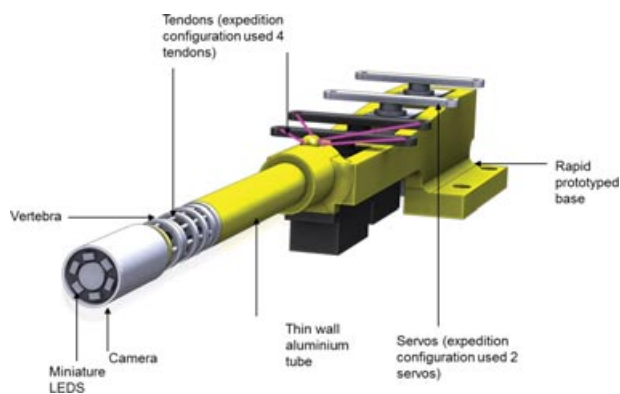
**Figure 16.** Render of the tendon arm with camera.

5.3. Snake Arm Camera

A snake arm camera was developed to explore the space between the pyramid blocking stones without having to carry out any further drilling of the stone. Therefore, it was made as small as possible (less than 8 mm diameter) while still potentially allowing a full 360° view of the chamber. The snake arm was constructed from several hollow plastic discs (vertebra) mounted onto a compliant central tube at precise intervals along the length of the tube (Figure 16). Tendons were attached to the outer portion of the vertebra in antagonistic pairs. When a tendon was placed under tension, the distance of the tendon mounting point to the center of the vertebra resulted in a torque applied to the vertebra and hence a bending motion. Applying tension to the other side of the antagonistic pair results in bending in the other direction. Four tendons were used, two in a horizontal plane and two in a vertical plane. Power and composite video cable was passed through the center of the compliant rubber tube. The head of the snake arm was mounted on a thin-walled steel tube, which in turn was mounted

on a rapid prototyped base. Miniature servos; were used to provide the torque to the tendons with a single servo controlling an antagonistic pair of tendons. Figure 16 illustrates four servos; this allowed independent actuation of the tendons or the capability to create a snake arm camera with two joints, however the system used here only made use of two servos for simplicity. This provided the snake arm with approximately +/−150° of movement range in the horizontal and vertical axis. A miniature camera with builtin LED's was mounted to the end of the snake arm. The camera had a 78° field of view, which, when combined with the movement of the snake arm, allowed approximately 95% of the chamber to be viewed. As there was no room for a focusing mechanism, the design used a wide-angle lens that compromised the depth of focus. The final depth of field allowed focus between approximately 2 and 12 cm from the tip of the camera. The inability to control camera exposure or gain settings resulted in a trade-off between too much and too little illumination; the amount of light in the camera view changed with camera position. Figure 17(A) illustrates the snake arm camera being deployed in a lab-based environment, and Figure 17(B) illustrates the snake arm immediately prior to entering the existing hole in the first blocking stone of the queen's chamber.

5.4. Drill Design

To explore past the second blocking stone (assuming it is a door of similar composition to the first blocking stone), it was necessary to develop a drill that could be deployed from the robot. The drill was designed to be as compact as possible, with a diameter less than 28 mm, to allow the drill itself to pass through the first blocking stone if a short drill piece is to be used, or if a deep hole is required in the second blocking stone. The drill was constructed from a drill motor, speed controller, and power supply all housed in a cross section of diameter less than 28 mm [Figure 18(A)].
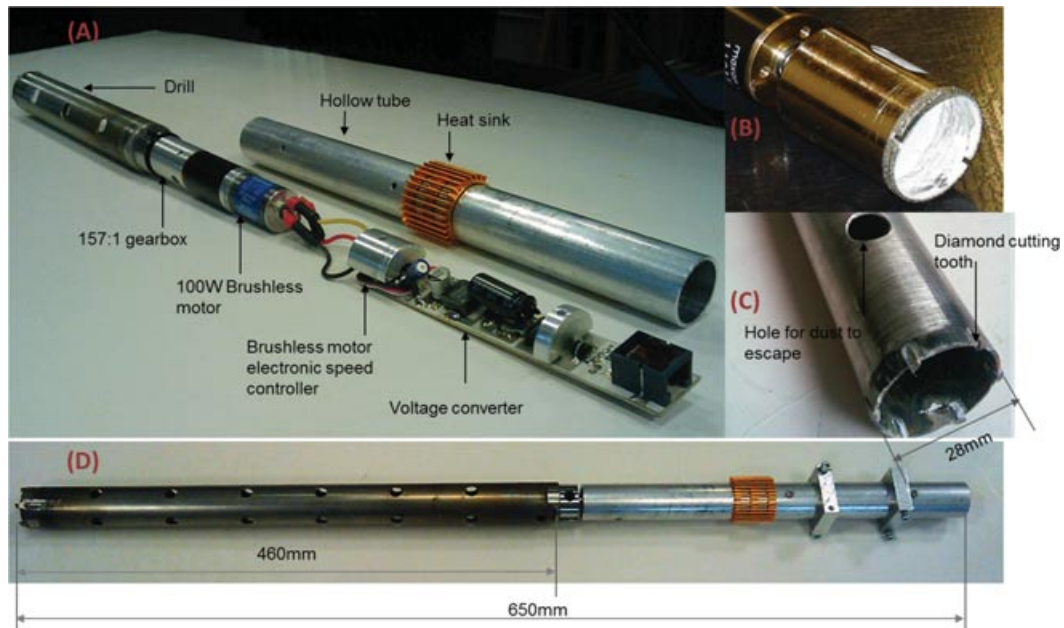
Figure 18. Images showing the drill test rig: (A) open drill, (B) standard diamond corer, (C) customized corer, (D) entire drill.

The voltage converter reduces 60 V to 12 V and an onboard brushless speed controller controls a 100 W brushless motor via a servo signal from the robot controller board. The motor output is reduced through a gear arrangement and transmitted to a screw attachment for the drill. The drill components are housed in an aluminum tube that is used as a heat sink along with an additional external heat sink. Established theory of coring into stone suggests a diamond corer to be the appropriate drill piece [Figure 18(B)]. However, trials in limestone with a standard diamond corer resulted in a buildup of stone dust that resulted in excessive drill forces. Indeed, this was even the case when drilling at an angle of 40°, where the dust was expected to fall out of the hole. Trials with a standard wood borer drill piece demonstrated that larger teeth allow the dust to escape and that a diamond tipped corer was not essential. The number of teeth resulted in high loading of the drill motor and high current usage. A custom drill piece was fabricated from a steel tube combined with teeth removed from a diamond tipped, toothed circle saw disc [Figure 18(C)]. This combination proved very successful at producing a smooth-edged hole while reducing the current required for the drill. Onboard the robot, the drill was capable of coring with a 460-mm-long corer and with this drill piece the overall drill length was 650 mm, the entire length of the rack [Figure 18(D)]. In actuality it is more likely that a shorter drill piece of 300 mm would be used to minimize robot weight and ensure the drill piece runs as concentrically as possible.

6. LAB-BASED PERFORMANCE TRIALS AND RESULTS

A series of laboratory-based tests were performed to ensure the performance of the robot meets the required specification: (i) An experiment was performed to measure the force required to push the front wheels over a step. The Djedi robot was modified to remove the rear carriage and place a force sensor between the rack and the ground. The tool carriage motor was used to drive the front carriage along the rack and over the step; the tool carriage motor and gearbox arrangement moved slowly to remove any dynamic effects and maintain a constant carriage speed for different size wheels. (ii) Drill tests were performed to measure the drill reaction force for various settings of drill speed and feed rate. A similar arrangement to that of the first experiment was used, which placed a force sensor between the rack and the ground. (iii) Locomotion and manoeuvering tests were performed in a specially constructed tunnel.

6.1. Step-Climbing Results

Four wheels of different radius were tested to measure the forces experienced during a 40 mm step climb. Wheels of radii 45, 50, 63, and 68 mm were used in the trials; when not used in this trial, these wheels were front and rear wheels of the robot at two different sizes—to allow adjustment of the tool height without modification of the robot structure. Figure 19 shows the experimental results of the trials. It is clear that the wheel radius of 45 mm requires a significantly higher force to be pushed over the step than the other wheel
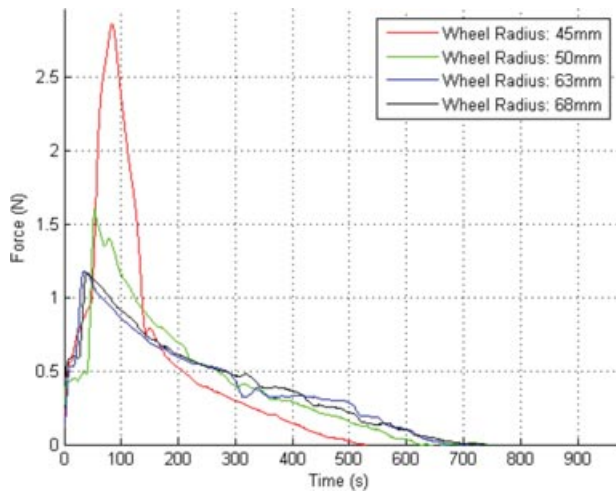
Figure 19. Force for different wheel diameters during the step climb.

sizes. A wheel radius of 50 mm reduced the required forces significantly, and the 63 and 68 mm wheels reduce the forces further. However, it is clear that the there is little improvement between 63 and 68 mm, validating the appropriateness of a wheel of radius 1.5 times the step height.

6.2. Locomotion and Steering Trials

A laboratory-based test shaft was constructed to allow robot manoeuvers to be attempted and practiced in a controlled environment [Figure 20(A)]. The test shaft consisted of a short entrance section, a 40 mm step after a 1 m climb, immediately followed by a 20 mm lateral step. Between 5 and 6 m there is a bend in the tunnel (for development of the northern shaft robots). Later, a larger test shaft in Egypt

was used to demonstrate and test the robots [Figure 20(B)], as discussed in Section 7.

Figure 21 illustrates a climbing manoeuver performed in the laboratory-based test shaft. The manoeuver required the robot to climb the shaft and traverse the floor and lateral step. The shaft width was set to 200 mm, less than the 210–240 mm that will be expected in the pyramid shafts. The reduced width makes navigating the lateral step challenging and is excellent driver training. Initially the robot starts completely on the left-hand side of the shaft. The robot performs a series of half-steps (the inchworm carriage does not move fully to the rear of the robot) designed to allow quick sideways movement over a number of steps. At each step, the extension of the brace actuators is adjusted to move the robot toward the right-hand side of the shaft. At frame "D" the robot has already moved to the middle of the shaft. At frame "I" the robot is on the right-hand side of the shaft and its wheel is just before a 40 mm step. The robot proceeds over the step and at frame "K" is just in front of a 20 mm lateral step. At frame "P" the rear wheel is just in front of the 40 mm step. Climbing over the 40 mm step for the rear wheel requires less force due to the increase in angle due to the front wheel on top of the step.

6.3. Drill Tests

It is important that the force exerted by the drill is minimized to prevent damage to the blocking stone and to ensure the robot maintains its grip in the shaft. Two variables control the drilling process: the drill rotational speed and the drill feed rate (how quickly the drill progresses into the stone). Figure 22 illustrates the drill force, measured through reaction force, for various drill settings. The hole is started
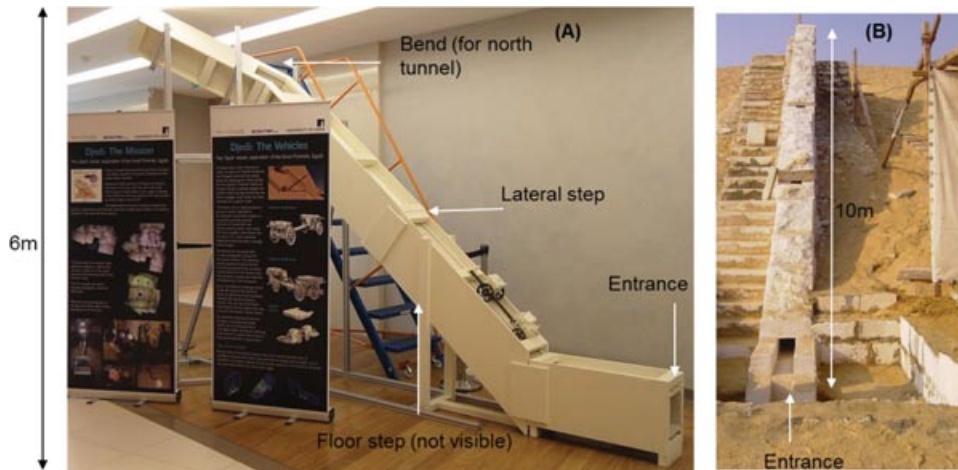
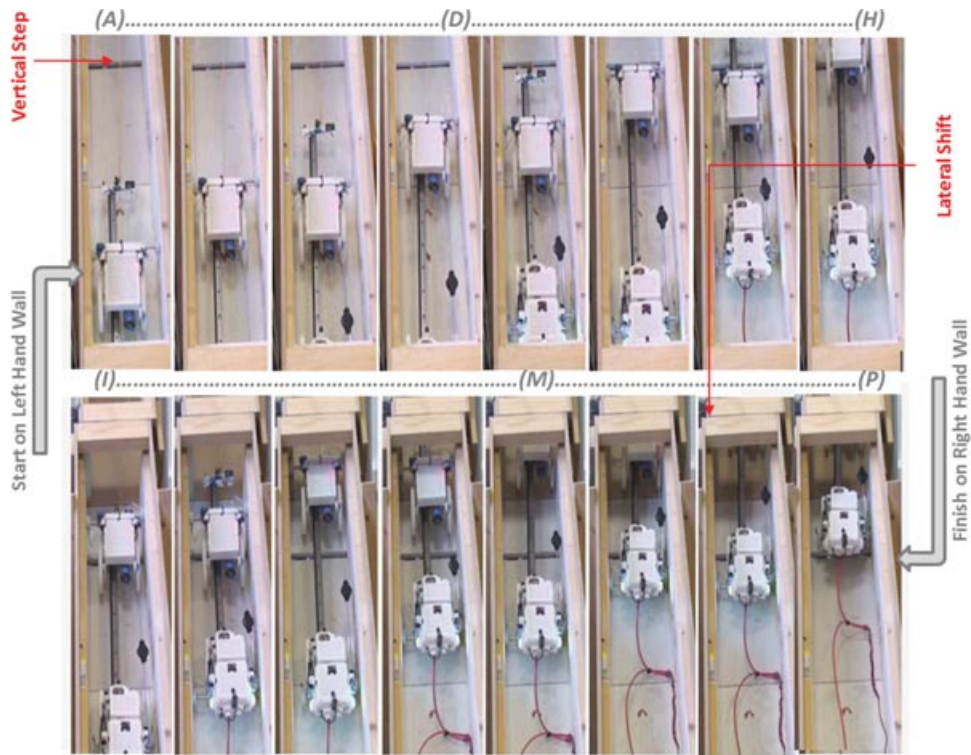**Figure 20.** The test tunnel built for deployment trials.

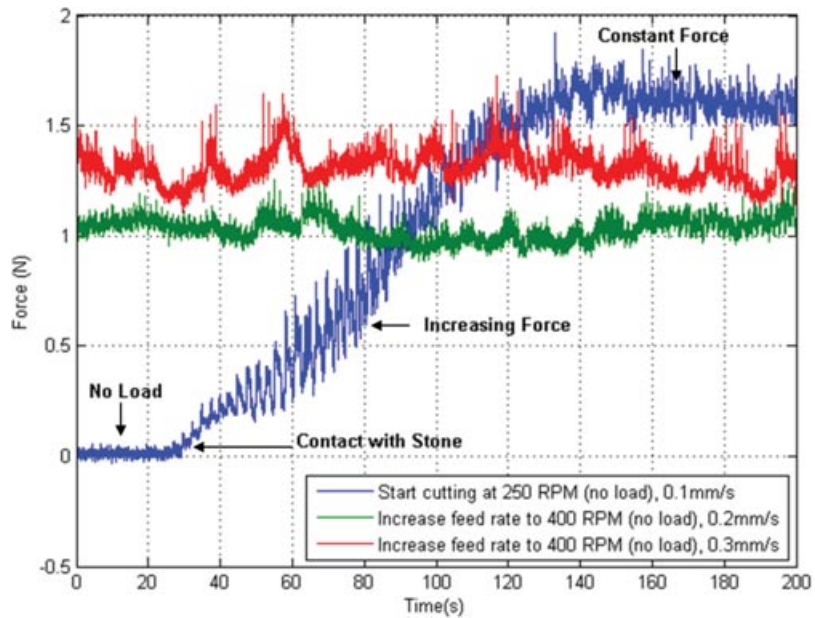**Figure 21.** Climbing sequence combined with a lateral shift.

Figure 22. Force exerted by the drill over time at different angular and linear velocities.

with settings of a low unloaded speed of 250 RPM and a low travel rate of 0.1 mm/s. There is a small amount of vibration when the drill is running in free space as recorded through the initial vibrations (this signal will also contain a small amount of electrical noise). As the drill comes into contact with the stone, the vibrations and force significantly increase, however there is not a large spike in force. The force applied gradually increases to a drill depth of around 1 mm, at which point the force value plateaus at around 1.6 N. The drill force for feed rates of 0.2 and 0.3 mm/s at 400 RPM no load (while the drill is in contact with the stone) are shown in Figure 21. Through an experimental process, the optimum drill settings to minimize force were found to be 400 RPM and 0.2 mm/s. As feed rate increases, so does the force applied. The plateau force for the low-speed, low-RPM trial exceeds the force for the other drill settings, however the initial drill settings are designed to minimize the kinetic energy on contact with the stone and therefore minimize the possibility of the drill contact producing a large shock load through the robot. Therefore, the drilling strategy is to approach the stone slowly at a low RPM. After 1 or 2 mm of drill travel, the settings will then be altered to first increase the drill rotational speed and then the feed rate to 0.2 mm/s. When the drill exits the stone (a hole has been drilled in the whole stone), the force drops momentarily and then rises to a value similar to the previous drilling force due to friction between the drill and the hole. During drilling the drill consumes 6 W of power at 250 RPM no load and a feed rate of 0.1 mm/s. At 400 RPM no load and a feed rate of 0.2 mm/s, 36 W of power is required. At the feed rate of 0.3 mm/s the drill consumes 48 W of power. There is a tradeoff between the time to drill the hole and thermal risk to the power converters and electronics. Tests were performed on the power converters for extended periods of time while supplying 36 W without them overheating. However, the thermal properties of the enclosed space within the shafts is difficult to predict, and temperature sensors in all the power supplies are essential to ensure overheating does not occur.

7. DEPLOYMENT WITHIN THE PYRAMID

Between 2006 and 2008, the Djedi team performed trials in a specially constructed test facility close to the pyramids in Egypt [Figure 20(B)]. The aim of these trials was to demonstrate the performance and reliability of the Djedi robot to gain permission to operate within the Great Pyramid. These trials offered an excellent opportunity to develop the robot technology to be robust to the heat and dust that is present around the pyramid. Initial trials suffered significant robot failures. The main cause of these failures was robustness of the electronics. To overcome these failings, the grounding of electrical circuit boards was redesigned and additional methods to cool the robots were introduced, including operating for limited periods of time, onboard cooling fans, and ensuring adequate ventilation space within the carriages.

In many ways the conditions of the Egypt test tunnel were more extreme than conditions in the pyramid itself, but the primary differences were (i) the heat outside the pyramid was significantly higher than inside, and (ii) there was more sand. Once these challenges were overcome, the Djedi robot successfully climbed the 10 m shaft in Egypt and drilled through two blocking stones, resulting in the team being granted access to the pyramid. The team carried out short surveys within the pyramid in the southern shaft in July and December 2009 and returned in May 2010 to complete the climb to the top of the shaft and carry out a video inspection of the small chamber behind the first blocking stone. This inspection took place on May 29th, 2010.

The short surveys of the shafts performed in 2009 allowed for simulation of a variety of failure modes close to the shaft entrance, such as a brace actuator malfunctioning and power cuts to all main systems. Several adjustments were made to the robot systems during these trials, primarily to improve the safety and ease at which the robot could be driven:

- Onboard lighting was adjusted to ensure lights were not pointed in direct camera view, and if unavoidably in line of sight they were automatically turned off when that camera was selected.
- Camera positioning was adjusted to ensure braces were viewed at all times and there was a clear view of the wheels and ground to avoid obstacles.
- The wires to the force sensors on the brace pads were repositioned to ensure they were not in contact with the wall.
- An automatic start up sequence was programmed onto the laptop to make starting the robot less complex and stressful for the operator.
- A dust cover was added to the inchworm carriage gears to shield them from dust.
- The tether cable was changed to a low weight and low friction custom-made cable.
- An emergency stop button was introduced on the laptop that stopped the robot but ensured it did not fall out of the shaft (cut power to inchworm carriage and actuate all braces).

7.1. A Successful Climb

In May 2010, the team returned with the aim of a full ascent of the shaft and a visual survey of what lay beyond the first blocking stone. On May 29th, the robot ascended the full length of the shaft carrying the snake arm camera and a servo-powered scoop as a nose attachment (to collect any items of interest on the tunnel floor, but it was not used in this deployment). Over the first 2 m of horizontal section and initial 40° angle, the robot was passively inserted using a specially designed rod that sits on the bodywork and allows the robot to be pushed from behind. The deployment

method worked perfectly and removed the need for the robot to climb through the transition from horizontal to 40°. At 30 m the robot encountered the lateral step and was successful in manoeuvering through it. At 59 m the robot encountered the 40 mm step in the floor, with the ramp deployed by the pyramid rover team still in position. This resulted in a very straightforward step ascent. Indeed, with the ramp in position the robot did not require its full step-climbing capability. However, it is possible the ramp could be displaced during robot operations, therefore the step-climbing capability of the robot may still prove to be crucial to the robot's success. The robot was demonstrated to be highly manoeverable within the shafts, particularly close to the blocking stone where the quality and smoothness of the shaft are very high. At the top of the shaft, the snake arm camera lined up perfectly with the existing hole, after a couple of sideways adjustments. The snake arm camera was successfully inserted through the blocking stone, allowing a full video survey of the space between the blocking stones.

Figure 23 shows camera images from the ascent. Figure 23(A) shows a view from the front carriage toward the back carriage and both rear braces against the tunnel wall. There is a spring-mounted camera at the rear of the robot that provided an excellent perspective for driving the robot while not impeding the initial transition from horizontal to 40° incline. Figure 23(B) is from the raised view of the spring camera and shows the front braces braced on the wall. Figure 23(C) shows the inchworm carriage midstride and the front braces retracted. Figure 23(D) shows the robot positioned toward the right side of the wall in preparation for traveling through the lateral step. Figure 23(E) shows the nose of the robot through the lateral step. Note the red mason's mark on the left-hand side. Figure 23(F) shows the inchworm carriage traveled through the lateral step. Figure 23(G) shows the robot through the lateral step. Note the lines on the side of the shaft caused by previous robot expeditions. Figure 23(H) shows the robot approaching the blocking stone. Figure 23(I) shows the robot aligning the bore scope with the previous hole. In Figure 21(G), note the slight roll of the robot in the shaft axis. This is due to the robot manoeuvering causing a twisting motion in the shaft (as described in Section 3). After a few forward steps, the robot roll had returned to the normal configuration of being aligned with the shaft floor.

7.2. Findings from Video Survey

The full results of the snake arm camera video survey are detailed in Hawass et al. (2010); these findings are summarized here.
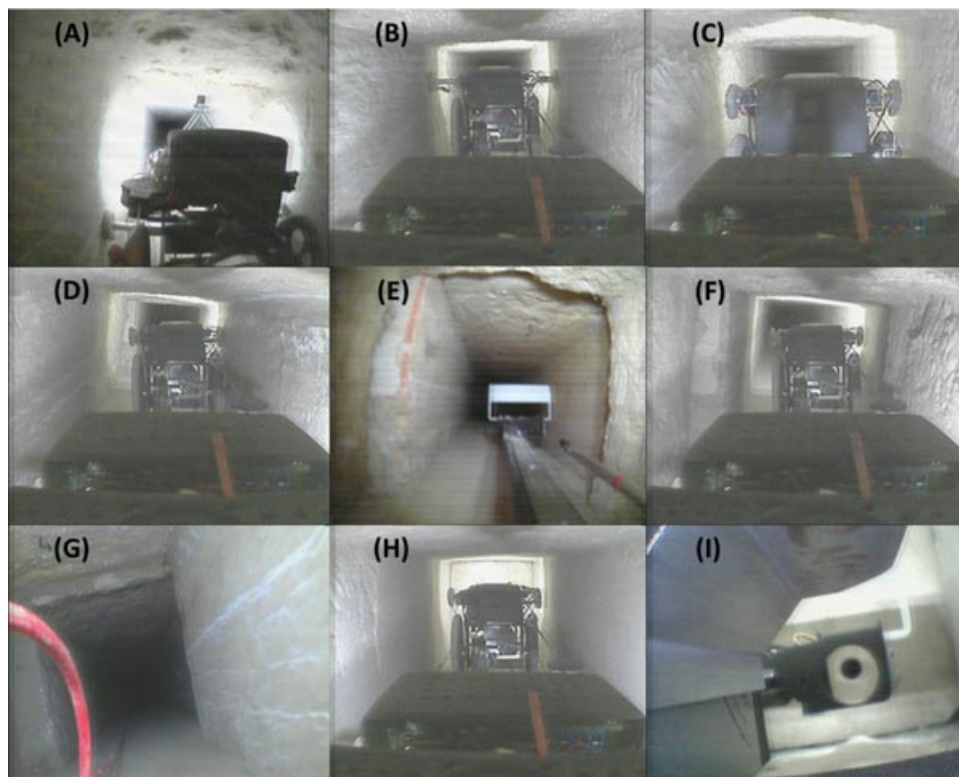
Figure 23. Camera images during the ascent in the shaft.
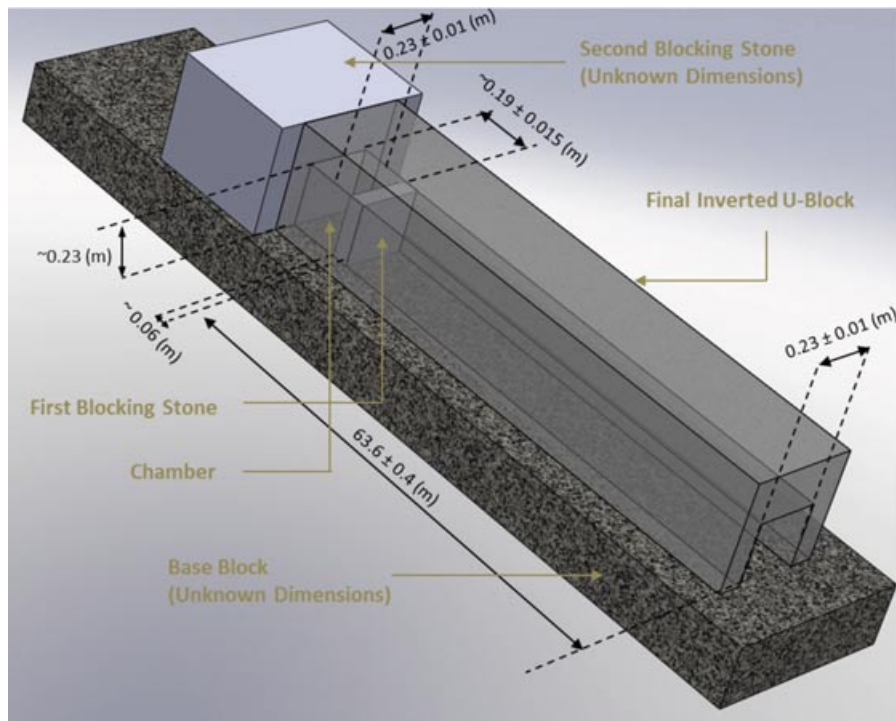
Figure 24. Construction of the chamber.

Most of the southern shaft is constructed from flat base blocks with inverted "U" blocks on top of them. Data from multiple sensors onboard the Djedi rover were used to reconstruct the chamber between the two blocking stones virtually (Figure 24). The position of the first blocking stone was measured by odometry on the rover (number of steps and length of each step) and verified by measuring the length of the umbilical cable. The position of the first blocking stone was found to be 63.6 ($\pm$0.4) m from the shaft entrance. The thickness of the first blocking stone appears to be approximately that found by Pyramid Rover, i.e., 60 mm, as obtained from markings on the snake camera as it passed through the hole.

### 7.2.1. Chamber Dimension Measurement

The final U-block in the shaft appears to be a fine white (probably Tura) limestone, carefully worked, as does the first blocking stone. There is a pair of converging cracks or veins on the ceiling of the U-block just behind the first blocking stone which appear to emerge at the front of the stone. This suggests that the walls and ceiling of the small chamber are formed by a continuation of this U-block. The chamber, therefore, appears to be formed by sliding the blocking stone, which is about 3 mm wider than the final U-block, down approximately 260 mm into the U-block until it rests on a small ledge. There is a diagonal chip or deliberate

chamfer where the blocking stone meets the ledge at the bottom right-hand side [Figure 25 (Left)]. The ledge on the right-hand side is obvious. The one on the left-hand side is not. There does not appear to be a ledge supporting the first blocking stone at the top. There is no obvious evidence that the first blocking stone is mortared into place on any side. There are two metal pins on the front face of the blocking stone. They are surrounded by a black material where they pass into the blocking stone. The green color of the pins suggests that they have a substantial copper content. The pins have been bent over flat against the blocking stone and have been broken off at an apparent weak point, which coincides with circular mortar patches. The left-hand pin was broken off naturally before the Upuaut missions; the right-hand pin was broken off by the Pyramid Rover. It is believed that both broken ends, around 12 mm long, were observed by the Djedi mission and will be collected in future Djedi missions.

The snake arm camera was able to look back on itself once inside the blocking stone space [Figure 25 (Right)]. The images revealed that the metal pins curve back on themselves. Figure 25(A) shows the copper pin facing down the shaft, and Figure 25(B) shows the corresponding hoop on the reverse. Figures 25(C) and (D) show the other pin and hoop pair.

The loops are very small and would only permit an approximately 3-mm-diameter object to pass through them.
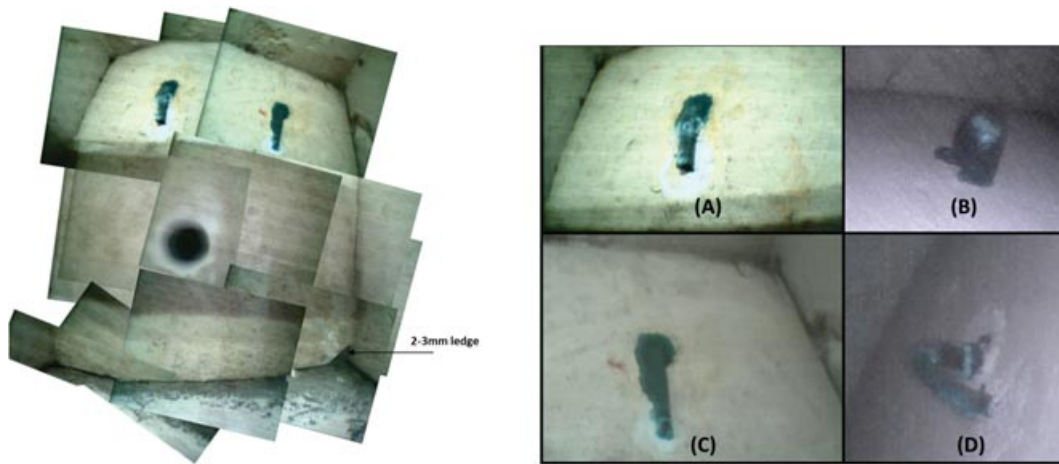
Figure 25. (Left) Images showing the chamfer where the blocking stone meets the ledge. (Right) (A) Front of left pin, (B) rear of left pin, (C) front of right pin, (D) rear of right pin showing mortar patches.

They do not appear to be very well positioned for functional purposes, as they are high up on the block.

The rear face of the first blocking stone is very carefully worked and is very flat. Other than the work around the ends of the pins, the block appears to be pristine except for a small lump of material or mark to its lower right-hand side. It is interesting to note that most of the debris behind the blocking stone has gathered on the right-hand side, as viewed from the back.

The floor of the chamber (looking toward the second blocking stone) has a red ochre mason's line running parallel to the shaft from just beyond the rear of the first blocking stone to the second blocking stone (Figure 26). There is also a black mark where the red line meets the second blocking stone. To the right of, and at approximately 45° to, the red line are three red ochre figures, possibly mason's marks or hieratic characters. The two main figures are similar to the hieratic number 21. There are also two other red marks on this side of the line.

7.3. Discussion on Robot Performance

The robot performed exceptionally well, climbing the full shaft length and deploying its bore scope camera through the existing hole. The initial specification (Section 1.4) detailed several key features that have been met or exceeded (for example, the drill depth of 460 mm well exceeds the desired depth of 360 mm). The cameras and lights operated very well, with the large number of cameras making manoeuvering the robot more straightforward. The camera resolution could be improved and at times electrical noise caused the pictures to degrade. The command and control systems worked well with the 2009 trials, proving invaluable in refining their quality; indeed, during the 2010 expedition several power cuts were encountered that required

the instigation of these procedures. At times the robot would tend to roll in the axis of the shaft due to the uneven floor and the high front brace actuator. The roll was soon corrected through several small steps in a straight line, however this was not ideal. The robot was paused after every 45 minutes of operation to allow it to cool down; this was not due to the presence of excessive heat, but rather as an additional safety precaution. However, this did slow the ascent down and in total it took approximately 6 hours to climb the shaft. Further endurance testing in a lab-based environment is required to increase confidence in robot systems and allow longer operation to speed up the ascent. Indeed, it is unclear whether the risk of continually powering up and down is lower than the risk of continuous operation.

7.4. Conclusions Drawn from Findings

The findings from the video survey provide valuable evidence toward the purpose and construction of the pyramid. For example, it has long been speculated what the purpose of the copper pins is and where they lead. This survey has shown that these pins are delicately curved into hoops and are too small for the mechanical purpose of lowering the blocking stone in place. As is often the case, the initial survey has resulted in more questions than answers:

- Why was it necessary to have such a large gap behind the blocking stone? If it was the intention to simply close the shaft without putting stress on this blocking stone, this could have been achieved by ensuring that there was just a small clearance between it and the second blocking stone, rather than the 190 mm clearance provided.
- What was the straight longitudinal mason's mark on the floor intended for? If it was a cutting mark, why was it not used?
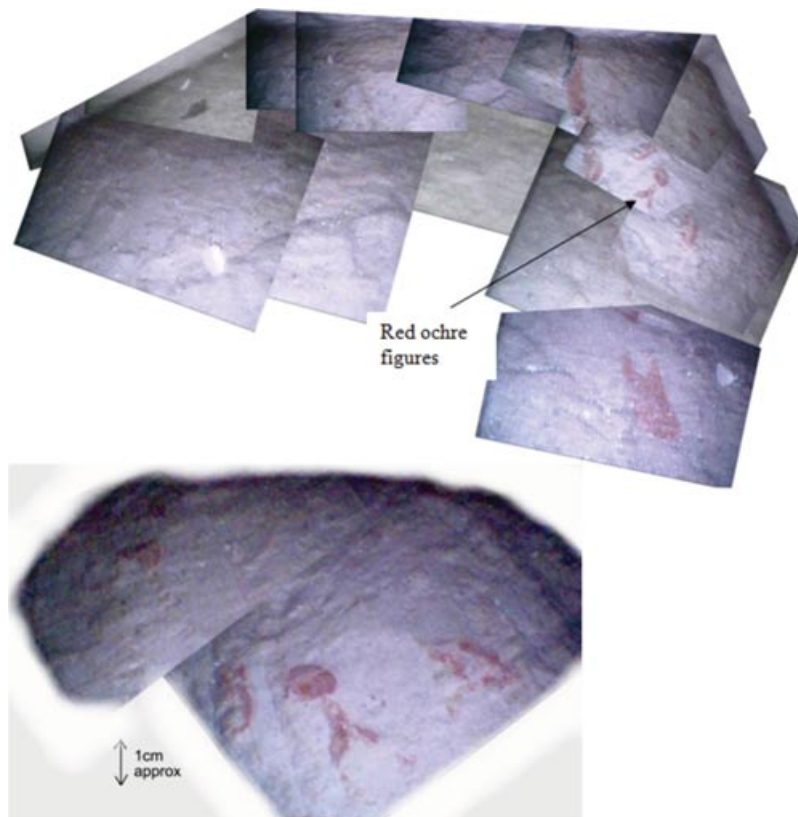
Figure 26. The ochre figures and mason's marks on the floor.

- What are the red symbols to the right of the longitudinal mason's mark?
- The second blocking stone appears to be a separate block from the shaft. Why was construction performed in this way? Is this a block laying across the end of the shaft? Or is it a blocking stone similar to the first one?

8. CONCLUSIONS AND FUTURE WORK

The Djedi robot operated as intended, and reached the top of the southern shaft. The locomotion system was successful in protecting the pyramid from damage, as no surface marks in the stone were observed after repeated climbs. The rapid prototyped bodywork proved to have sufficient strength to endure the forces experienced during manoeuvering in the shaft. The use of four brace pads (two in contact during climbing) proved sufficient to maintain traction on the surface of the shaft in spite of the shaft walls being dusty and uneven in places. The ramp in front of the large step (as left by a previous expedition) reduced the need for robot step climbing ability. A reduced requirement for step climbing would allow a smaller front wheel, which in turn would allow a reduction in the size of the front carriage and slightly larger tool deployment depth. The mechanical power generated from the locomotion motor proved to be sufficient to climb the shaft, although toward the top of the shaft the robot occasionally had to take a couple of steps backward to slacken the cable and move it slightly to reduce friction. Therefore, an increase in motor torque would be desirable for a greater factor of safety and to ensure a successful climb. However, an increase in motor torque would either result in additional weight or lower climbing speed through a lower gear ratio. The primary drawback of the inchworm locomotion approach is the climbing speed. It took around four hours to climb the shaft (including delays for planning the locomotion at particular points). This time is acceptable when one or two ascents are planned, but if multiple tasks involving multiple tools are required, the ascent time would become a serious issue. The bore scope was deployed and viewed almost the full interior of the chamber for the first time. Many interesting and useful shaft features were observed that will help to fulfill the primary objective of the mission, which is to determine the purpose of the shafts and blocking stones. However, the evidence is not conclusive, and as expected, further work is required as soon as it becomes practical. The next steps should include:

1. Further image processing, converting the 2D images into 3D to allow researchers to consider the significance of the features.
2. Further analysis and interpretation of the red ochre markings.
3. Modifications to the snake arm camera, taking into account the geometry and the coloring of the stones that is now known about the chamber, including the ability to see the whole block/wall in order to take more precise measurements of the features. Also the ability to get close to joints to view them accurately. Now that the positioning of the existing hole is known, it is possible to make the snake camera slightly larger, allowing higher resolution and more illumination.
4. Deployment of a high-definition video camera onboard the rover to survey fine details of the shaft.
5. Development of a miniature sonic surveyor tool to determine the thickness of the second blocking stone, and drilling of the second blocking stone, if appropriate.
6. Deployment of variants of the robot technology to explore the northern shaft.

ACKNOWLEDGMENTS

REFERENCES

Bertetto, A., & Ruggiu, M. (2001). In-pipe inch-worm pneumatic flexible robot. In Advanced Intelligent Mechatronics, 2001, Proceedings of the 2001 IEEE/ASME International Conference (Vol. 2, pp. 1226–1231). IEEE.

Buehler, M., Battaglia, R., Cocosco, A., Hawker, G., Sarkis, J., & Yamazaki, K. (1998). Scout: A simple quadruped that walks, climbs, & runs. In Robotics and Automation, 1998. Proceedings of the 1998 IEEE International Conference (Vol. 2, pp. 1707–1712). IEEE.

Choi, C., Park, B., & Jung, S. (2010). The design and analysis of a feeder pipe inspection robot with an automatic pipe tracking system. IEEE/ASME Transactions on Mechatronics, 15(5), 736–745.

Choi, H., & Ryew, S. (2002). Robotic system with active steering capability for internal inspection of urban gas pipelines. Mechatronics, 12(5), 713–736.

Fujiwara, S., Kanehara, R., Okada, T., & Sanemori, T. (1994). Development of an articulated multi-vehicle robot for monitoring and testing in pipe. Journal of the Robotics Society of Japan, 12(2), 318–327.

Fukuda, T., Hosokai, H., & Otsuka, M. (1987). Autonomous pipeline inspection and maintenance robot with inch worm mobile mechanism. In Robotics and Automation. Proceedings of the 1987 IEEE International Conference (Vol. 4, pp. 539–544). IEEE.

Gantenbrink, R. (1999). The upuaut project. URL: http://www.cheops. org.

Hawass, Z. (2002). The secret doors inside the Great Pyramid. http://www.drhawass.com/events/mystery-hidden-doors-inside-great-pyramid-0 Last accessed 20 Feb 2013.

Hawass, Z., Whitehead, S., Ng, T., Richardson, R., Pickering, A., Rhodes, S., Grieve, R., Hildred, A., Tayoubi, M., & Breitner, R. (2010). First report: Video survey of the southern shaft of the queen's chamber in the great pyramid. Annales du Service des Antiquits de l'Egypte, 84, 203–216.

Hirai, K., Hirose, M., Haikawa, Y., & Takenaka, T. (1998). The development of honda humanoid robot. In Robotics and Automation, 1998. Proceedings. 1998 IEEE International Conference (Vol. 2, pp. 1321–1326). IEEE.

Hirose, S., Yoneda, K., Arai, K., & Ibe, T. (1994). Design of a quadruped walking vehicle for dynamic walking and stair climbing. Advanced Robotics, 9(2), 107–124.

Huang, H., Yan, J., & Cheng, T. (2010). Development and fuzzy control of a pipe inspection robot. IEEE Transactions on Industrial Electronics, 57(3), 1088–1095.

Kawaguchi, Y., Yoshida, I., Kurumatani, H., Kikuta, T., & Yamada, Y. (1995). Internal pipe inspection robot. In Robotics and Automation, 1995. Proceedings, 1995 IEEE International Conference (Vol. 1, pp. 857–862). IEEE.

Kim, D., Park, C., Kim, H., & Kim, S. (2009). Force adjustment of an active pipe inspection robot. In ICCAS-SICE, 2009 (pp. 3792–3797). IEEE.

Lim, J., Park, H., Moon, S., & Kim, B. (2007). Pneumatic robot based on inchworm motion for small diameter pipe inspection. In Robotics and Biomimetics, 2007. ROBIO 2007. IEEE International Conference (pp. 330–335). IEEE.

Lu, C., Huang, H., Yan, J., & Cheng, T. (2007). Development of a pipe inspection robot. In Industrial Electronics Society, 2007, IECON 2007, 33rd Annual Conference of the IEEE (pp. 626–631). IEEE.

Moore, E., & Buehler, M. (2001). Stable stair climbing in a simple hexapod robot. Technical report, DTIC Document.

Okada, T., & Kanade, T. (1987). A three-wheeled self-adjusting vehicle in a pipe, ferret-1. The International Journal of Robotics Research, 6(4), 60–75.

Roh, S., & Choi, H. (2005). Differential-drive in-pipe robot for moving inside urban gas pipelines. IEEE Transactions on Robotics, 21(1), 1–17.

Saranli, U., Buehler, M., & Koditschek, D. (2001). Rhex: A simple and highly mobile hexapod robot. The International Journal of Robotics Research, 20(7), 616–631.

Schempf, H., Mutschler, E., Gavaert, A., Skoptsov, G., & Crowley, W. (2010). Visual and nondestructive evaluation inspection of live gas mains using the explorer family of pipe robots. Journal of Field Robotics, 27(3), 217–249.

Shin, B., Bang, Y., Choi, S., & Lee, S. (2010). Inchworm-like robot locomotion using segmented solenoids. In Advanced Intelligent Mechatronics (AIM), 2010 IEEE/ASME International Conference (pp. 367–372). IEEE.

Taguchi, K., & Kawarazaki, N. (1997). Development of in-pipe inspection robot for small radius pipelines. Journal of the Robotics Society of Japan, 15(2), 230–235.

Talebi, S., Buehler, M., & Papadopoulos, E. (2000). Towards dynamic step climbing for a quadruped robot with compliant legs. In 3rd Int. Conf. on Climbing and Walking Robots, Madrid, Spain. John Wiley & Sons.

Thueer, T., Krebs, A., & Siegwart, R. (2006). Comprehensive locomotion performance evaluation of all-terrain robots. In Intelligent Robots and Systems, 2006 IEEE/RSJ International Conference (pp. 4260–4265). IEEE.

Xu, F., & Wang, X. (2008). Design and experiments on a new wheel-based cable climbing robot. In Advanced Intelligent Mechatronics, 2008. AIM 2008. IEEE/ASME International Conference (pp. 418–423). IEEE.

Yoon, K., & Park, Y. (2010). Pipe inspection robot actuated by using compressed air. In Advanced Intelligent Mechatronics (AIM), 2010 IEEE/ASME International Conference (pp. 1345–1349). IEEE.